ISSN 1331-7210 (Print)
ISSN 2718-322X (Online)

Engineering Power

BULLETIN OF THE CROATIAN ACADEMY OF ENGINEERING Vol. 19(3) 2024

EDITOR-IN-CHIEF'S WORD

Dear Readers,

Engineering today stands at the forefront of addressing the critical challenges of energy efficiency, environmental sustainability, and technological advancement. This issue of Engineering Power reflects this imperative by presenting original scientific and technical contributions that align with the global demand for smarter, more sustainable systems and practices.

The papers featured in this edition are representative of the international and interdisciplinary scope of contemporary engineering research. They highlight the evolving role of engineering not only as a driver of innovation but also as a key enabler of energy transition, resource optimization, and climate resilience. Across diverse sectors—including energy systems, manufacturing processes, and thermal technologies—these contributions emphasize the need for integrated solutions based on rigorous analysis, novel design approaches, and a deep understanding of physical principles.

By fostering dialogue between academic research and practical application, Engineering Power continues to support the mission of the Croatian Academy of Engineering to promote excellence, encourage collaboration, and address the pressing technical issues of our time. We trust that this issue will inspire further research, critical thought, and real-world innovation in the pursuit of engineering solutions that contribute to a more sustainable and efficient future.

Editor-in-Chief
Vedran Mornar, President of the Croatian Academy of Engineering

EDITOR'S WORD

Dear Readers,

The new issue of Engineering Power jorunal, edited by Prof. Neven Duić, PhD, brings us three papers from the SDEWES conference series. The broad spectrum of topics related to environmental protection, which is typical for the SDEWES conference series is also reflected in the original scientific papers in this issue. Heat recovery devices, energy-efficient and sustainable solutions in the printing process and cold storage are topics which may be of interest to you. We hope you enjoy reading this issue.

Editor
Bruno Zelić, Vice-President of the Croatian Academy of Engineering

FOREWORD

With a broad vision of integrating various systems for long-term sustainability, the international conference series on the sustainable development of energy, water, and environmental frameworks was launched at the beginning of the 21st century. Now in its third decade since the first gathering in Dubrovnik, Croatia, which set the foundation for the series in 2002, the need for this integrated perspective has never been more pressing. Utilizing surplus from one system as a resource for another at the right moment is one of the most crucial challenges in preserving the Earth's essential support systems. Enhancing the efficiency of interconnected systems–spanning electricity, heating, cooling, transportation, water management, waste treatment, industrial operations, construction, forestry, and agriculture–serves as a key strategy for reducing environmental impact while allowing development to progress. This holistic approach to sustainability offers significant opportunities for accelerating efforts toward reducing carbon emissions and tackling climate change.

The field of engineering is well-positioned to address sustainability challenges, but it must move beyond rigid disciplinary boundaries and embrace the need for equipping future professionals with diverse competencies. The technical solutions required to lower environmental impact while retaining the conveniences of modern life are inherently interdisciplinary, drawing from electrical, mechanical, information, civil, chemical, food-related, and other engineering disciplines, as well as architecture, economics, agriculture, and forestry.

This edition presents three forward-looking innovations in technology and methodology for assessing sustainability that could contribute to a more environmentally responsible way of life.

The first case examines the windcatcher [1], a natural ventilation system with a dual-channel rotating air scoop for airflow in all wind conditions. It integrates passive energy solutions and a heat recovery system, achieving 95% airflow retention and 15% efficiency.

The second study addresses sustainability in flexographic printing, introducing a life-cycle-based methodology to analyze energy flows and improve environmental impact assessments for optimized energy use [2].

The final study explores cold thermal storage, evaluating capsule arrangements for energy efficiency [3]. The face-centered cubic layout boosts packing density by 22% and reduces charging duration by 21%, enhancing thermal transfer.

References:

[1] J. Li, J. Calautit i C. Jimenez-Bescos, »A novel arrangement of metal fin heat recovery device in a dual channel wind scoop windcatcher system for reducing the building energy demand in temperate climates,« Engineering Power, svez. 19, br. 3, 2024.

[2] A. Babu, A. Piacentino, A. Bicego, L. Fratini, V. Lo Brano, G. Ingarao i D. Zorzi, »A systematic method for identifying energy-efficient and sustainable solutions in the Flexographic printing process,« Engineering Power, svez. 19, br. 3, 2024.

[3] Y. Zhang, X. Zhai, Z. Zhou i X. Wang, »Numerical Exploration of Flow and Thermal Performance in Packed-Bed Cold Storage Enhanced by Structured PCM Capsule Layouts,« Engineering Power, svez. 19, br. 3, 2024.

Guest Editor
Neven Duić, University of Zagreb, Faculty of Mechanical Engineering and Naval Architecture

CONTENT

Jiaxiang Li[1], John Calautit[2], Carlos Jimenez-Bescos[3]

A novel arrangement of metal fin heat recovery device in a dual channel wind scoop windcatcher system for reducing the building energy demand in temperate climates

[1]University of Nottingham, Nottingham, UK, jiaxiang.li@nottingham.ac.uk
[2]University of Nottingham, Nottingham, UK, ezzjkc@exmail.nottingham.ac.uk
[3]University of Westminster, London, UK, c.jimenezbescos@westminster.ac.uk

Abstract

The windcatcher, an innovative natural ventilation apparatus, facilitates the provision of fresh air and ensures indoor thermal comfort under suitable external conditions. This research introduces an advanced dual-channel windcatcher system that employs a rotary wind scoop, offering ventilation regardless of wind direction and incorporating passive and low-energy technologies. A cost-effective, low-pressure loss heat recovery design for the rotary scoop windcatcher was devised, featuring stationary fins between the supply and return channels. This design allows for heat recovery in the natural ventilation system, with heat being consistently transferred through the metallic fins. A Computational Fluid Dynamics (CFD) model, corroborated by experimental data, was adapted to assess ventilation performance and heat recovery efficiency. The findings revealed that the windcatcher system, equipped with a heat recovery (HR) unit, maintained over 95% of its initial ventilation rate. Furthermore, a heat recovery efficiency exceeding 15% was attained by utilizing a one-meter-long heat recovery unit in this study.

***Keywords**: Windcatcher, CFD, heat recovery, natural ventilation, wind tunnel*

1. Introduction

As energy prices continue to rise and concerns over global warming intensify, researchers are exploring ways to increase energy efficiency across various sectors. One sector that could make a significant contribution to achieving a sustainable energy economy is the built environment. The construction and built environment industries are responsible for over 40% of the direct and indirect global carbon emissions (He, Yang et al. 2014). Heating, Ventilation and Air Conditioning (HVAC) systems are responsible for over half of the energy consumption in buildings, with air conditioning being one of the fastest-growing energy users in the built environment (Pérez-Lombard, Ortiz et al. 2008, Liu, Justo Alonso et al. 2022). This places a significant burden on the electricity grid in many parts of the world. Therefore, researchers are seeking sustainable and cost-effective solutions that provide good indoor thermal comfort and air quality to building occupants while minimizing the use of air-conditioning (Jomehzadeh, Hussen et al. 2020).

Natural ventilation is an attractive solution and has been the focus of many research studies. But natural ventilation is typically insufficient to provide the required indoor thermal comfort in unfavourable hot and cold climatic conditions. Thus, researchers are looking for sustainable and economical solutions to provide building occupants with good indoor thermal comfort and air quality while minimizing the use of air-conditioners, such as combining natural ventilation with other passive/low-energy strategies, including solar heating, heat recovery, cooling and dehumidification (Jomehzadeh, Hussen et al. 2020, Zhang, Yang et al. 2021, Bamdad, Matour et al. 2022).

Heat recovery systems were proposed in the ventilation system but mainly in mechanically ventilated buildings. In the natural ventilation system, the windcatcher is a suitable natural ventilation device for heat recovery integrations with both supply and return channels. Much research investigated the heat recovery system in windcatcher systems using heat pipes (Calautit, O'Connor et al. 2016, Chaudhry, Calautit et al. 2017, Calautit, Tien et al. 2020, Barreto, Qu et al. 2022), solid tubes (Liu, Jimenez-Bescos et al. 2022) and thermal mass wheels (Calautit, O'Connor et al. 2019, Calautit, O'Connor et al. 2020). Heat pipes are suitable for low-resistance systems driven

by wind, increasing room temperatures by 2.8°C (Mahon, Friedrich et al. 2022). However, the high price of the heat pipes would result in a high capital cost and maintenance cost. A case study in the UK demonstrated that integrating heat recovery into natural ventilation systems can effectively provide fresh air with minimal energy use (Dorizas, Samuel et al. 2018). Moreover, the pressure loss through the system results in a low ventilation rate in natural wind conditions and additional fans are necessary for the system.

In addition, the traditional multidirectional ventilation device can not provide a stable heat recovery, because the heat exchange between supply and return channels was not always stable (Mahon, Friedrich et al. 2022). The heat recovery in a conventional four-sided windcatcher was investigated, but the frequent switching of inlet and outlet would decrease the heat recovery efficiency (Liu, Jimenez-Bescos et al. 2022, Mahon, Friedrich et al. 2022).

The supply-to-return area ratio in the traditional four-sided windcatcher is not constant which might be switched between 1 and 3. At the condition with a supply-to-return area ratio of 3, the heat recovery between the supply and return channels is not balanced and the recovery efficiency was not maximized. As shown in Figure 1, the varying wind direction would also cause reverse flow and the heat recovery performance will be decreased (Khan, Su et al. 2008). Moreover, the channels on the opposite sides were not adjacent which further limited the efficiency of heat recovery. Thus, although effective heat recovery with so many limitations is something better than nothing, investigating a suitable design to overcome the limitation of traditional passive heat recovery is necessary for low-carbon natural ventilation in buildings and industries.

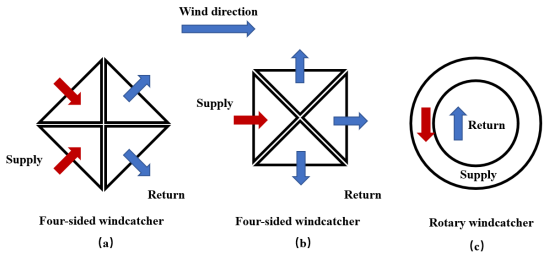

Fig. 1. Comparison of the ventilation airflow direction in a typical multi-directional windcatcher and the proposed rotary windcatcher (a) wind direction from an edge in four-sided windcatcher (45° from the face) (b) wind direction from a face in four-sided windcatcher (c) in rotary scoop windcatcher

Heat recovery systems are vital for energy conservation in buildings, capturing and reusing waste heat to enhance thermal efficiency and significantly reduce energy consumption (Calautit, O'Connor et al. 2020). A case study in the UK demonstrated that integrating heat recovery into natural ventilation systems can effectively provide fresh air with minimal energy use (Dorizas, Samuel et al. 2018). In windcatcher natural ventilation systems, common heat recovery technologies include heat pipes (Calautit, O'Connor et al. 2016, Liu, Jimenez-Bescos et al. 2022, Mahon, Friedrich et al. 2022) and thermal wheels (Calautit, O'Connor et al. 2019, Calautit, O'Connor et al. 2020). Heat pipes are suitable for low-resistance systems driven by wind (Barreto, Qu et al. 2022), increasing room temperatures by 4.5°C (Calautit, O'Connor et al. 2016) and 2.8°C (Mahon, Friedrich et al. 2022).

The aim of this study is to advance the development of a heat recovery unit within the rotary scoop windcatcher with low-pressure loss. This aim will be achieved through the utilization of Computational Fluid Dynamic (CFD) simulations. This research will encompass three distinct yet interconnected objectives: (1) experimental validation of the model; (2) evaluation of the ventilation performance of the windcatcher, with integrated heat recovery unit; and (3) assessment of the overall heat recovery performance of the unit.

To achieve the first objective, experimental validation will be conducted to ensure the accuracy and reliability of the model. Subsequently, the performance of the integrated windcatcher with a heat recovery unit will be evaluated. Lastly, the heat recovery unit's overall performance will be assessed, taking into account various factors such as the rate of heat recovery, temperature efficiency, and pressure loss. This research will advance the understanding of heat recovery units within rotary scoop windcatchers, providing insights into their performance and limitations.

2. Method

This section discussed the method which included numerical CFD modelling using ANSYS Fluent software and experimental wind tunnel testing to validate the model. The data obtained from the simulations and experiments were used to evaluate the ventilation performance and heat recovery efficiency of the device.

2.1. Proposed system model and prototype

In prior research, the potential for heat recovery integration in building natural ventilation was explored through the proposal of a novel windcatcher design (Figure 2). This innovative design offers independent ventilation, irrespective of the prevailing wind direction (Li, Calautit et al. 2023). The windcatcher design incorporates a rotary wind scoop and a concentric tube arrangement that ensures fixed supply and return channels. Consequently, the impact of fluctuating wind directions is effectively eliminated.

The unique characteristics of this windcatcher design make it suitable for the application of a passive heat recovery device. This device, which utilizes metal fins to capture heat from the return duct, can be seamlessly integrated into the windcatcher structure to provide efficient, low-cost heat recovery. The metal fins enable the transfer of heat from the outgoing air to the incoming air, thereby recovering heat that would otherwise be lost.

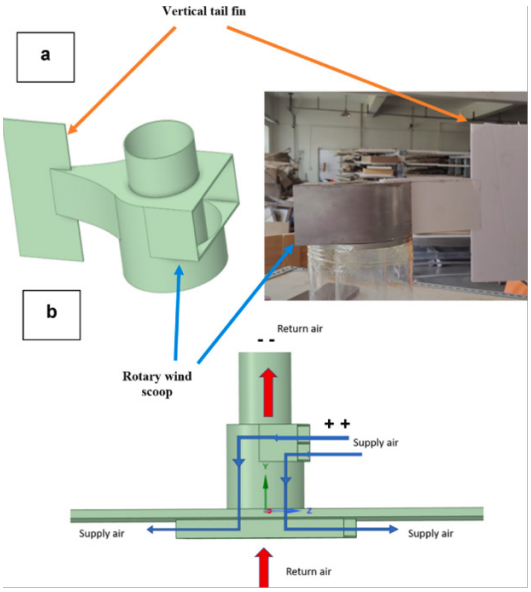

Fig. 2. (a) Proposed rotary scoop windcatcher for passive heat recovery integration (Li, Calautit et al. 2023) and (b) operation

In the initial windcatcher design, the supply and return channels were separated by the internal tube. However, the limited contact surface area posed a challenge to achieving efficient heat recovery. To address this issue, metal fins were inserted into the internal tube to increase the contact area, resulting in the creation of a heat recovery unit (Figure 3).

The heat recovery unit was fabricated using aluminium fins with a thickness of 1 mm. The fins had a length of 95 mm, with 62mm on the supply side and 32mm on the return side. The fins were arranged at an angle of 12 degrees, and a total of 72 fins were used. To simulate the heat transfer process, aluminium panels with a thickness of 1mm were employed in the numerical simulations. The use of aluminium panels was favoured due to their superior strength, lower thermal conductivity than steel, and lower cost than copper. After decreasing the thickness of the metal panels to approximately 1mm, the thermal resistance of the panels was negligible, and the heat transfer efficiency was primarily influenced by the convection heat transfer coefficient between the air and the metal panels. The height of the fins was varied between 0.5m and 1m for evaluating the heat recovery efficiency.

The validated windcatcher tubes had external and internal diameters of 450mm and 300mm, respectively. The ventilation performance of the windcatcher was previously validated in research (Li, Calautit et al. 2023), and this study focused on evaluating the performance of the heat recovery unit.

The incorporation of the metal fins heat recovery unit in the windcatcher system offers a promising approach for reducing the building energy demand. The results of this study could have significant implications for sustainable building design, particularly in temperate climates, where natural ventilation is commonly used, and efficient heat recovery systems are in high demand.

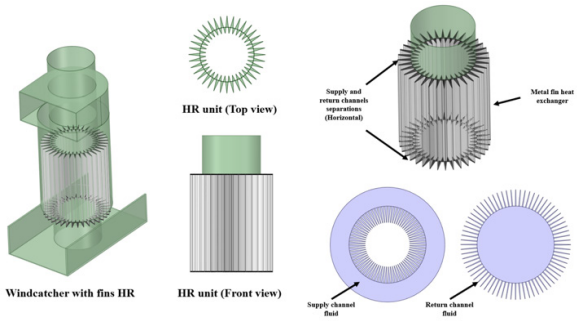

Fig. 3. Windcatcher with metal fins heat recovery unit and the supply & return air channels

2.2. Experimental wind tunnel testing

To evaluate the performance of the windcatcher prototype, a test room cube with the dimensions 1.2m x 1.2m was constructed, using 50mm thick insulation board to ensure thermal insulation (Figure 4). To prevent airflow short-circuiting and ensure good air circulation inside the test room, two L-shape anti-short circuit devices (ASCD) were installed, as per previous research (Li, Calautit et al. 2023). The windcatcher prototype was placed in the centre of the test room.

A 4m long open wind tunnel (Figure 4) was constructed for testing the windcatcher ventilation rate. The wind tunnel was equipped with a contraction section, screen mesh, and honeycomb flow conditioners, as described in previous research (Li, Calautit et al. 2023). The screen mesh and flow conditioners were used to establish a turbulent flow from the industrial fans, creating a stable airflow suitable for evaluating the CFD model, as reported in previous research (Li, Calautit et al. 2023).

The wind speed profiles measured from the outlet of the wind tunnel were used as the inlet boundary conditions for the CFD simulations, providing a reliable representation of the actual airflow conditions. The resulting data were used to evaluate the ventilation performance of the windcatcher and to optimize its design for maximum efficiency.

The use of a dedicated test room and wind tunnel facility allowed for controlled experimental conditions and provided valuable insights into the performance of the windcatcher prototype. The results of this study have significant implications for sustainable building design, offering a promising approach to reducing energy consumption and associated greenhouse gas emissions.

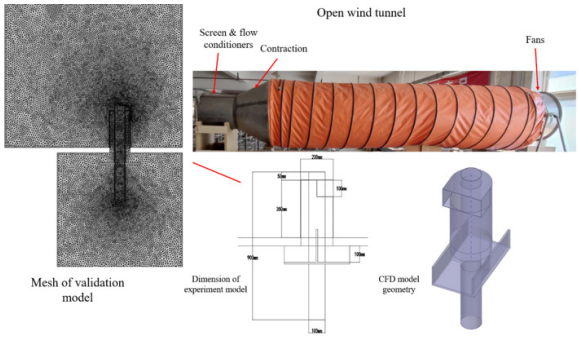

Fig. 4. Wind tunnel and CFD model set-up and the dimension of the model

2.3. CFD modelling

In this research, the performance of the suggested system is assessed through the implementation of Computational Fluid Dynamics (CFD) simulations. The commercial software, FLUENT, is employed for conducting the airflow simulations. Concurrently, the three-dimensional model is developed utilizing Spaceclaim, which is integrated into the Ansys Workbench software environment.

The mass, momentum and energy equations are solved for the airflow within this model. The Reynolds-averaged Navier-Stokes and k-epsilon equations are applied, in accordance with previous research (Li, Calautit et al. 2023). A second-order upwind scheme is utilized to discretize all transport equations. The widely adopted Semi-implicit Method for Pressure-Linked Equations (SIMPLE) segregated pressure-based algorithm solver is implemented for turbulent airflow simulations. The governing equations for mass (eqn.1), momentum (eqn.2), and k and epsilon (eqn.3 and 4) are incorporated within the model. The detailed parameters in the simulation model were presented in Table 1.

$$\frac{\partial \rho}{\partial t} + \nabla \cdot (\rho u) = 0 \quad (1)$$

$$\frac{\partial \rho}{\partial t} + \nabla \cdot (\rho u u) = -\nabla p + \rho g + \nabla \cdot (u \nabla u) - \nabla \cdot \tau_t \quad (2)$$

$$\frac{\partial (\rho k)}{\partial t} + \nabla \cdot (\rho u k) = \nabla \times [(\mu + \frac{\mu_t}{\sigma_k}) \nabla k] + P_k - \rho \varepsilon \quad (3)$$

$$\frac{\partial (\rho \varepsilon)}{\partial t} + \nabla \cdot (\rho u \varepsilon) = \nabla \cdot [(\mu + \frac{\mu_t}{\sigma_\varepsilon}) \nabla \varepsilon] + \frac{c_{1\varepsilon} P_k}{k} \varepsilon - C_{2\varepsilon} \rho \frac{\varepsilon^2}{k} \quad (4)$$

In order to test the heat recovery potential of the windcatcher, the governing energy equation (5) was added to the CFD simulation method.

$$\frac{\partial (\rho e)}{\partial t} + \nabla \cdot (\rho e u) = \nabla \cdot (k_{eff} \nabla T) - \nabla \cdot (\sum_i h_i j_i) \quad (5)$$

where: is velocity (m/s), t is time (s), ρ is density (kg/s), g is gravitational acceleration (m/s²), p is pressure (Pa), τt is stress tensor of the turbulence stresses (Pa), μ is dynamic molecular viscosity (Pa·s), μ_t is turbulent viscosity (Pa·s), is turbulent production of kinetic energy (kg·m^{-1}·s^{-3}), e is specific internal energy (J/kg), $C_{1\varepsilon}$ and $C_{2\varepsilon}$ are empirical constants (dimensionless), keff is effective heat conductivity (W/(m·K)), hi is specific enthalpy of fluid (J/kg), T is air temperature (K), ji is mass flux (kg/(m²·s))

To simplify, the heat recovery efficiency of the windcatcher and the ventilation performance of the windcatcher were evaluated separately. The mesh element number of the heat recovery simulation of a 0.5m and 1m long heat recovery unit were 2.16 million and 3.42 million, respectively. The mesh elements of the windcatcher with and without a heat recovery unit were 12.6 million and 4.22 million, respectively. Three different models with elements of 0.22 million, 0.88 million and 4.22 million were used for the mesh sensitivity analysis and the ventilation performance difference between the three mesh sizes was ignorable, with an average difference of 0.5%. However, the model with highest mesh number, 4.22 million, was selected in this research with higher resolution for a better visulization performance.

Table 1. CFD settings and boundary conditions in accordance with previous research (Li, Calautit et al. 2023).

Term	Value and settings
Inlet	
Velocity (m/s)	0-3 (profiled wind speed for validation)
	1-7 (constant wind speed for optimizations)
Initial Gauge Pressure (Pa)	0
Specification Method	k-epsilon RNG
Outlet	
Gauge Pressure (Pa)	0 (atmospheric)
Wall	
Shear Condition	No slip
Roughness Models	Standard
Roughness Height	0
Roughness Constant	0.5
Converged residuals	
Continuity / k / Epsilon	0.001
X/Y/Z velocity	0.0001

In the heat recovery evaluation, the external supply air temperature was 0°C (273 K) and the internal return air temperature was 27°C (300 K). The heat recovery efficiency was evaluated by the internal energy difference between the supply and return air and heat flux through the metal fins.

3. Results and discussion

3.1. Model validation

The experimental validation results, together with the velocity contour, are depicted in Figure 5. In the case of the scaled prototype, fresh air was supplied at rates ranging from 1.7 L/s/m² to 9.18 L/s/m², taking into account outdoor wind speeds varying between 0.5 m/s and 2.5 m/s. The mean discrepancy in the ventilation rate between the Computational Fluid Dynamics (CFD) simulation and the experimental data was 0.156 L/s/m², with an average variance of 4.5%. An observed linear relationship emerged between the average wind speed and the ventilation rate. The investigation showed that the difference in ventilation rate between the CFD model, which integrated profiled wind from the open wind tunnel, and the homogeneous environment wind under comparable average wind speeds was insignificant.

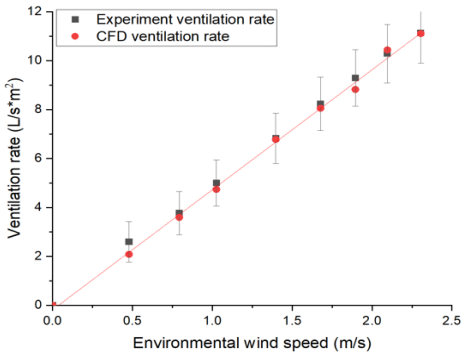

(c)

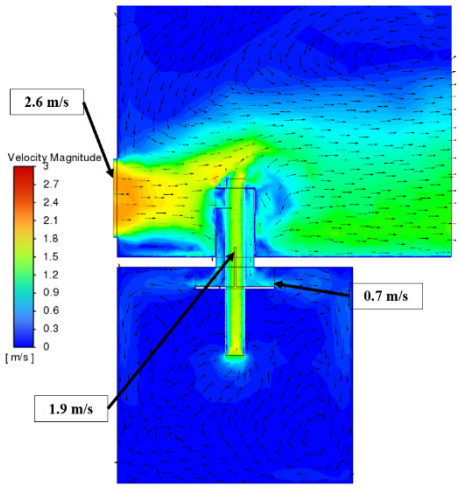

Fig. 5. Experimental and CFD results comparison and the velocity contour of the validation model

3.2. Ventilation performance

The ventilation performance of the windcatcher model without the HR unit and the model with a 0.5m long HR unit are shown in Figure 6. Similar linear relationships between the ventilation rate and the environment were achieved, and the HR unit only decreased 4.5% of the total ventilation rate. As the fins only increased the contact surface area without affecting the section area in the long channel, the overall ventilation rate was not significantly affected (Figure 6). The high ventilation rate of the initial windcatcher remained for a sufficient fresh air supply, and a low-pressure loss increment in the 0.5m long HR unit provides the potential of installing a longer HR unit in the windcatcher system.

3.3. Heat transfer efficiency

The heat transfer rate and efficiency of the 0.5m HR unit are shown in Figure 7. and the HR efficiency of HR units with different lengths is shown in Figure 9. With the increase of mass flow rate, the heat transfer rate increased steadily, but the HR efficiency was slightly decreased. A higher airflow velocity around the heat recovery surface increased the convectional heat transfer coefficient but the convectional heat transfer coefficient was not proportional to the airflow velocity and the increase of the convectional heat transfer coefficient was decreased with the increase of airflow velocity. Thus, the HR efficiency was decreased from 10% to 6.5%. HR efficiency of about 15% was achieved in a windcatcher with a 1m long HR unit which would decrease to 14% at a higher ventilation rate condition. However, in most cases, the ventilation rate of the ventilation system would not be increased to over 300 L/s which requires an environment wind speed of over 10 m/s. Thus, the heat recovery efficiency would remain at a higher level.

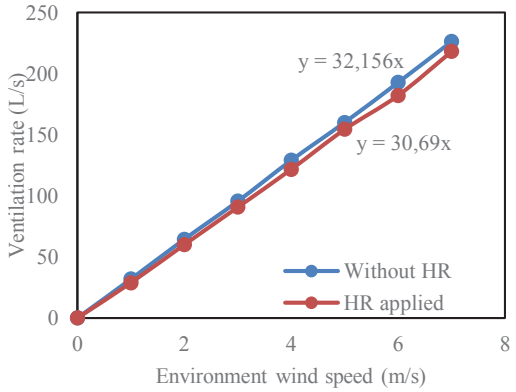

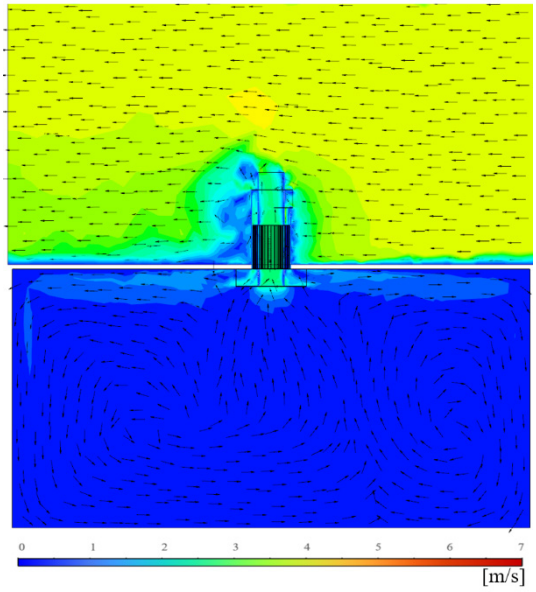

Fig. 6. *Ventilation performance and velocity contour of the windcatcher model with and without HR unit (0.5m long fins)*

The temperature contour with a 27 temperature difference between supply and return air in the 1m heat recovery unit and the velocity contour under a high airflow rate are shown in Figure 8. A heat recovery unit with an efficiency of 15%, could increase the supply air temperature by 4 under a 27temperature difference between supply and return air. This temperature increase is higher than a windcatcher heat recovery system using heat pipes, increas-

ing room temperatures by 2.8°C (Mahon, Friedrich et al. 2022), and the cost of flat metal panels is much lower than the cost of heat pipes which the heat recovery windcatchers in this research commercially viable. The airflow velocity between the fins was decreased, and the pressure loss of the system was increased, which decreased the total ventilation rate of the windcatcher.

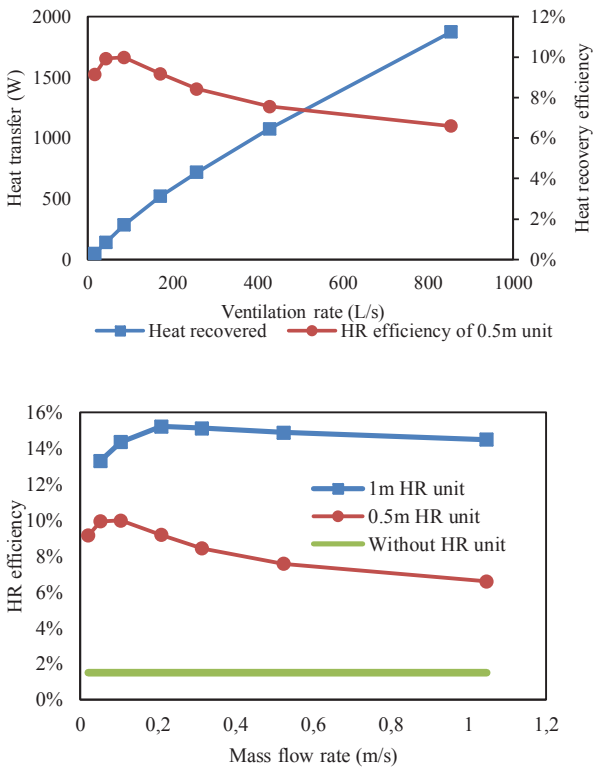

Fig. 7. *Heat transferred through metal fins and the heat recovery efficiency of a 0.5m heat recovery unit after increasing the ventilation rate, and heat recovery efficiency of 0.5m and 1m heat recovery units*

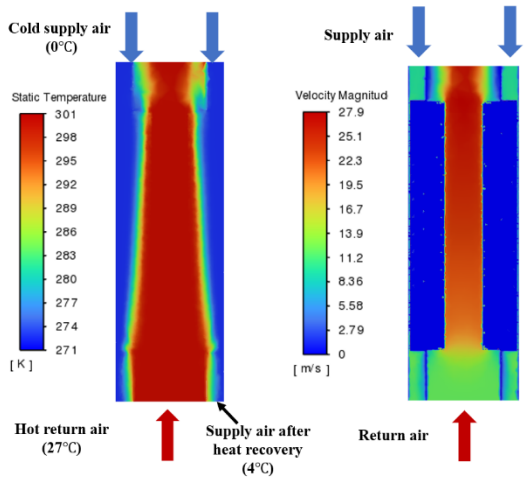

Fig. 8. Temperature and velocity contour in the 1m heat recovery unit

4. Conclusion

In this study, a passive heat recovery system utilizing low-pressure loss metal fins was proposed for integration into a rotary scoop windcatcher. The initial scaled windcatcher model was assessed through wind tunnel experiments and Computational Fluid Dynamics (CFD) simulations. Subsequently, a full-scale windcatcher model was optimized based on the scaled model, with the heat recovery unit applied to the full-scale configuration. Ventilation performance and heat recovery efficiency were evaluated using CFD simulations.

The full-scale windcatcher demonstrated a ventilation rate exceeding 160 L/s when subjected to an outdoor wind speed of 5 m/s. The ventilation rate loss incurred by a 0.5 m heat recovery unit amounted to a mere 4.5%, maintaining a high ventilation rate of over 150 L/s under the same outdoor wind speed. The heat recovery efficiency of 0.5 m and 1 m heat recovery units approximated 9% and 15%, respectively, with the potential for further enhancement by employing longer heat recovery units. A 4°C increase in supply air temperature was achieved by a windcatcher with a 1 m heat recovery unit under a 27°C temperature differential.

In this preliminary investigation, a simple design and operation principle were employed for the heat recovery system. Heat recovery efficiency was intentionally limited to preserve high ventilation efficiency. The contact surface-to-volume ratio in the channels can be further augmented by increasing the number of fins and obstructing the space beyond the fins. Given that ventilation efficiency was not significantly impacted by the heat recovery unit, the unit's length can be extended to attain higher heat recovery efficiency without compromising ventilation efficiency. Furthermore, the windcatcher's height is typically elevated to capture wind at higher speeds and minimize interference with the building's edge. Sufficient space for a heat recovery unit is available, allowing for an overall heat recovery efficiency increase that satisfies both designers and occupants.

Future research should evaluate the metal fins heat recovery device using wind tunnel experiments. Additionally, optimizing the metal fins and windcatcher geometry will be essential for attaining higher ventilation rates and heat recovery efficiency. The windcatcher used in this research has a diameter of about 0.5m. In the further application of this windcatcher, the dimensions of the windcatcher should range from 0.2m to 1m, which is similar to the application of a wind turbine with different sizes based on the ventilation demand. The passive solar heating, passive cooling using evaporative cooling, and passive dehumidification design in the windcatcher system should also be investigated in further research.

5. Nomenclature

e	Specific internal energy (J/kg K)
Gb	Generation of turbulence kinetic energy due to buoyancy
Gk	Generation of turbulence kinetic energy due to mean velocity gradients
h_i	Specific enthalpy of fluid (J/kg)
j_i	Mass flux (kg/s)
k_{eff}	Effective heat conductivity (W/m K)
m	Mass of fluid(kg)
p	Pressure (Pa)
P_k	Turbulent production of kinetic energy
ΔQ	Heat flux through the heat recovery unit (W)
σ_k	Turbulence model constant of *k*
σ_ε	Turbulence model constant of ε
t	Time (s)
T	Air temperature (K)
u	Velocity (m/s)
$\overline{V}$	Average airflow velocity in the return duct (m/s)
V_c	Airflow velocity in the centre of the return duct (m/s)
αk	Inverse effective Prandtl numbers for *k*
α_ε	Inverse effective Prandtl numbers for ε
μ	Dynamic molecular viscosity (Pa s)
μ_t	Turbulent viscosity(m^2/s)
ρ	Density (kg/m^3)
τ_t	Divergence of the turbulence stress
ASCD	Anti-short circuit device
CFD	Computational Fluid Dynamic
HVAC	Heating, ventilation and air-conditioning
HR	Heat Recovery

6. References

Bamdad, K., S. Matour, N. Izadyar and T. Law (2022). "SIntroducing extended natural ventilation index for buildings under the present and future changing climates." Building and Environment: 109688.

Barreto, G., K. Qu, Y. Wang, M. Iten and S. Riffat (2022). "An innovative window heat recovery (WHR) system with heat pipe technology: Analytical, CFD, experimental analysis and building retrofit performance." Energy Reports **8**: 3289-3305.

Calautit, J., D. O'Connor, S. Shahzad, K. Calautit and B. Hughes (2019). "Numerical and experimental analysis of a natural ventilation windcatcher with passive heat recovery for mild-cold climates." Energy Procedia **158**: 3125-3130.

Calautit, J. K., D. O'Connor and B. R. Hughes (2016). "A natural ventilation wind tower with heat pipe heat recovery for cold climates." Renewable Energy **87**: 1088-1104.

Calautit, J. K., D. O'Connor, P. W. Tien, S. Wei, C. A. J. Pantua and B. Hughes (2020). "Development of a natural ventilation windcatcher with passive heat recovery wheel for mild-cold climates: CFD and experimental analysis." Renewable Energy **160**: 465-482.

Calautit, J. K., P. W. Tien, S. Wei, K. Calautit and B. Hughes (2020). "Numerical and experimental investigation of the indoor air quality and thermal comfort performance of a low energy cooling windcatcher with heat pipes and extended surfaces." Renewable Energy **145**: 744-756.

Chaudhry, H. N., J. K. Calautit and B. R. Hughes (2017). "Optimisation and analysis of a heat pipe assisted low-energy passive cooling system." Energy and Buildings **143**: 220-233.

Dorizas, P. V., S. Samuel, M. Dejan, Y. Keqin, M.-M. Dimitris and L. Tom (2018). "Performance of a natural ventilation system with heat recovery in UK classrooms: An experimental study." Energy and Buildings **179**: 278-291.

He, B.-j., L. Yang, M. Ye, B. Mou and Y. Zhou (2014). "Overview of rural building energy efficiency in China." Energy Policy **69**: 385-396.

Jomehzadeh, F., H. M. Hussen, J. K. Calautit, P. Nejat and M. S. Ferwati (2020). "Natural ventilation by windcatcher (Badgir): A review on the impacts of geometry, microclimate and macroclimate." Energy and Buildings **226**: 110396.

Khan, N., Y. Su and S. B. Riffat (2008). "A review on wind driven ventilation techniques." Energy and Buildings **40**(8): 1586-1604.

Li, J., J. Calautit, C. Jimenez-Bescos and S. Riffat (2023). "Experimental and numerical evaluation of a novel dual-channel windcatcher with a rotary scoop for energy-saving technology integration." Building and Environment: 110018.

Li, J., J. K. Calautit and C. Jimenez-Bescos (2023). "Experiment and numerical investigation of a novel flap fin louver windcatcher for multi-directional natural ventilation and passive technology integration." Building and Environment **242**: 110429.

Liu, M., C. Jimenez-Bescos and J. Calautit (2022). "CFD investigation of a natural ventilation wind tower system with solid tube banks heat recovery for mild-cold climate." Journal of Building Engineering **45**: 103570.

Liu, P., M. Justo Alonso and H. M. Mathisen (2022). "Heat recovery ventilation design limitations due to LHC for different ventilation strategies in ZEB." Building and Environment **224**: 109542.

Mahon, H., D. Friedrich and B. Hughes (2022). "Wind tunnel test and numerical study of a multi-sided wind tower with horizontal heat pipes." Energy **260**: 125118.

Pérez-Lombard, L., J. Ortiz and C. Pout (2008). "A review on buildings energy consumption information." Energy and Buildings **40**(3): 394-398.

Zhang, H., D. Yang, V. W. Y. Tam, Y. Tao, G. Zhang, S. Setunge and L. Shi (2021). "A critical review of combined natural ventilation techniques in sustainable buildings." Renewable and Sustainable Energy Reviews **141**: 110795.

Anson Babu[1], Antonio Piacentino[1], Alessandro Bicego[2], Livan Fratini[1], Valerio Lo Brano[1], Giuseppe Ingarao[1], Diego Zorzi[2]

A systematic method for identifying energy-efficient and sustainable solutions in the Flexographic printing process

[1]University of Palermo, Department of Engineering, Palermo, Italy
[2]Uteco Converting S.p.A., Product Innovation Department, Verona, Italy

Abstract

The growing demand for printing on packaging products from end-users increases energy demand, raw materials consumption, and direct emissions in the flexible packaging print and conversion industries. Innovative and energy-efficient solutions must be implemented in the flexographic printing process for long-term energy savings and reducing the environmental impact. However, the existing studies on flexographic printing processes in industries lack a detailed, in-depth analysis of the energy, material, and emissions study at a process sub-unit level. Moreover, a systematic method is needed to investigate the influence of process parameters, waste heat potential, and auxiliary units in the flexographic printing processes to explore future research possibilities. Therefore, a Life cycle-oriented in-depth approach is presented for the use phase of flexographic printing machine at a process sub-unit level. A detailed measurement test plan is presented to identify the unknown flows through the machine for in-depth Life cycle analysis. The paper concludes with possible recommendations for energy savings and sustainability solutions for flexographic processes in the future.

***Keywords**: Energy efficiency, sustainability, flexographic printing, life cycle analysis, waste heat recovery.*

1. Introduction

The global energy demand is increasing due to the increasing population and rapid industrialisation. The manufacturing sector of industries not only consumes energy and resources but also generates significant levels of emissions and waste into the atmosphere. Industries account for 37% of global energy use and are directly responsible for a quarter of the global CO2 emissions, which lead to serious environmental issues such as global warming and climate change [1]. To mitigate these impacts, industries have started implementing energy efficiency measures by adopting sustainable and innovative solutions in manufacturing processes. Government policies and measures that aim to improve energy efficiency in industries also help reduce emissions and environmental impact to a great extent. Energy optimisation in the industrial sector not only improves sustainability performance but also reduces manufacturing costs.

Flexographic printing is widely used for producing high-quality prints in the packaging and labelling industry due to its faster production speed, extremely versatile print process, and in-line converting flexibility. The growth of the flexographic printing market has been driven by the rising demand for high-quality printed packaging products, especially in the food, beverages, pharmaceuticals, and cosmetics sectors. According to recent reports, the market size was valued at approximately USD 8.5 billion in 2022 and is expected to grow at a compound annual growth rate (CAGR) of over 14% from 2023 to 2029 [2]. However, this growth creates several challenges, particularly concerning the environmental impact of the flexographic printing process due to higher energy demand, resource consumption, and direct emissions. To address this issue, the Printing and Packaging Industries have also started adopting the concepts of sustainability and energy efficiency principles in flexographic printing. The main driving forces behind implementing energy-efficient, sustainable, and innovative solutions in industries include stringent government policies, environmental concerns, and the long-term economic benefits achievable in the manufacturing of flexographic printed products.

1.1 Flexographic printing technology

Flexographic printing technology uses a flexible printing plate, usually a polymer or rubber, mounted on a cylinder to transfer ink to a substrate (web). A wide variety of substrates can be used in flexographic printing, such as paper, plastic, and aluminium. The plate cylinder holds the ink graphics plate (flexo plate) to be printed on the substrate. At first, the ink is transported from the ink tray to the anilox roller, which is then transferred to the graphics of the flexible plate. The doctor blade removes the excess ink from the anilox roller before it transfers ink to the flexible plate. This ensures the precise amount of ink transfer and improves the print quality. The substrate passes between the plate cylinder and the impression cylinder to transfer the print, and sufficient pressure for printing the web is provided by the impression cylinder (**Fig. 1.**)

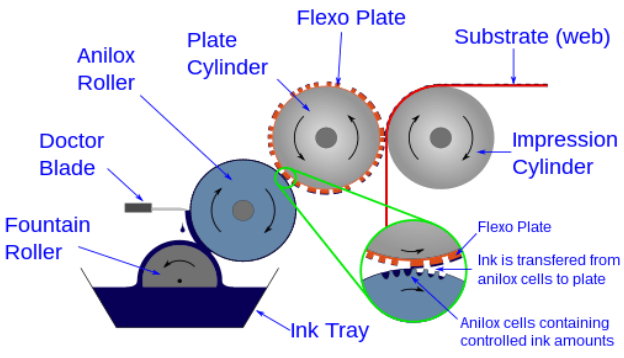

Fig. 1. Flexographic printing technology [3]

1.2 Processes involved in flexographic printing.

The main processes involved in manufacturing a flexographic printed substrate are shown in **Fig.2**. At first, the loaded substrate on the machine is unwound and then fed into the main printing unit. Inks of distinct colours needed for printing are pumped into the main printing unit. Once the ink is transferred from the plate roller to the substrate by flexographic printing, wet ink on the substrate needs to be converted from liquid to solid phase. The curing of inks is done by the drying process, which generally consumes a lot of energy and produces significant emissions into the atmosphere. Depending on the final product requirements and ink type, several types of drying technologies can be used. The hot printed substrate coming out from the drying section undergoes a cooling process; usually, chilled rollers are used to reduce the substrate temperature by absorbing the excess heat present in it. Finally, the final product of the flexographic printed substrate is re-winded and ready for the customers. The operator checks the quality of the printed substrate, and if needed, the process parameters are adjusted for the required print quality. Depending on the requirements of users, post-printing processes such as coating and laminating can be done on the final product, if needed.

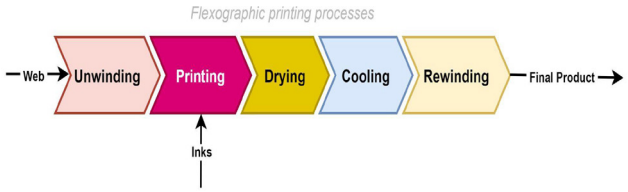

Fig.2. Main Process in Flexographic Printing

1.3 Drying process

The drying process in flexographic printing is the main source of direct emissions with significant energy consumption. The product quality of the printed substrate depends not only on the visual aspect but also on the drying quality. The presence of residual solvents in the printed substrate must be strictly avoided especially when printing food packaging and pharmaceutical products. The drying quality in the flexographic process depends on many factors, such as the ink type, ink viscosity, substrate material, production speed, and the kind of drying mechanism used. The primary focus will be optimising the drying process to ensure energy efficiency and sustainability in flexographic printing. **Fig.3** shows the common types of drying processes used in flexographic printing.

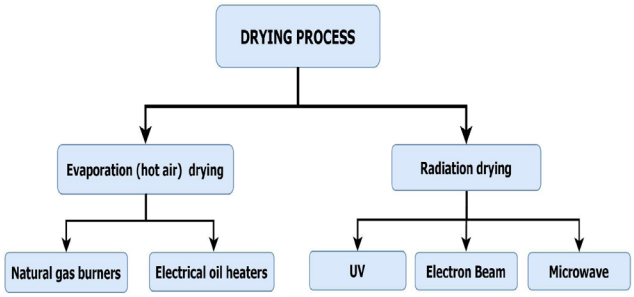

Fig. 3. Main types of Drying in Flexographic printing

Evaporation drying

Evaporation drying is the most commonly used drying method in the flexographic printing process for water- or solvent-based inks, but it consumes a significant amount of thermal and electrical energy. Using ventilation fans, hot air is blown into the printed substrate over both sides with nozzles in the drying tunnel. The solvents or water present in the ink evaporates quickly, and the remaining ink components create a dry film on the printed substrate. Natural gas burners and electrical oil heaters are generally used to heat the air to the required temperature needed for the drying process. The temperature and speed of hot air are the main process parameters that affect the drying rate in hot air drying. The higher the temperature and speed of air, the higher the drying rate, but it also increases thermal and electrical energy consumption [4]. Therefore, an optimum value of hot air temperature and fan speed must be set for proper drying quality as well as for energy savings. The choice of a suitable nozzle is also a key factor for optimising the drying process.

The experimental research conducted by Hardisty used the infra-red technique to identify the drying curves of inks. [5]. The drying curves consist of a constant rate period and a falling rate period separated by a critical point (**Fig. 4.**) [6]. Around 80% of the solvents in the printed web get evaporated in the early stages of drying at a constant rate. In the final stages of drying, more time is required to remove even smaller quantities of solvents from the web, and the trend of falling rate period is experienced. These insights show that during the falling rate period, air temperature and speed have less influence on the drying rate and thus provide a future research scope for energy savings in the drying process.

A study conducted by Burak et al. [7] investigated the heat and mass transfer coefficients in the evaporative drying of ink films with impinging air jets. The comparison of the theoretical results for the falling rate and constant rate period obtained in the study with other experimental and theoretical data showed a satisfactory result, especially for drying time.

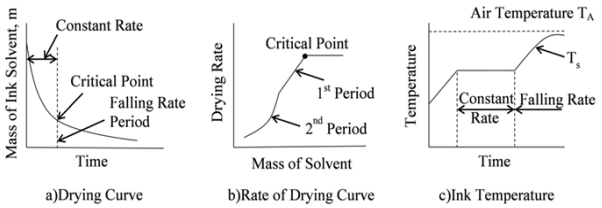

Fig. 4. Drying curve characteristics of inks [6,7]

The solvent-based inks evaporate at lower temperatures and require less energy for ink curing than water-based inks. Water-based inks generally limit printing production speed due to their lower drying rate. Higher air temperature and flow rate are needed for the proper drying of water-based inks. Special attention must be paid while printing with water-based inks because the substrate could also lose material properties due to overheating. Due to higher

humidity content in the exhaust air leaving the drying chamber, direct recirculation of the exhaust air into the drying process is limited in the case of water-based inks.

On the other hand, a part of the exhaust air is always recirculated into the drying process in the case of solvent-based inks, and the remaining inlet air is always compensated with fresh air or ventilation air. This reduces the thermal energy demand of the drying process when printing with solvent-based inks. However, using solvent-based inks instead of water-based inks is not the best solution when considering the environmental impact.

The solvent-based inks contain Volatile organic compounds (VOC) such as ethanol, ethyl acetate, and isopropyl alcohol, which are the main sources of direct emissions in the flexographic printing process. The drying process of solvent-based ink contributes around 75% of the total VOC emissions in the printing industry. Due to their highly volatile nature, some of the solvents evaporate directly from the ink tank at room temperature. The exhaust air leaving the drying section containing VOC must undergo a treatment process before expelling air into the atmosphere [8].

A material and energy flow study conducted by Irina et al. [9] in a flexible printing and packaging plant adopted the Integrated pollution prevention and control (IPPC) methods such as replacing solvent-based with water-based inks, upgrading the ventilation system, and improving the lighting system. The results showed a decrease in VOC emissions of 92.5% and a reduction in energy consumption by 21.5% in the industry.

Radiation drying

Radiation drying is used in flexographic printing industries to accelerate production speed by reducing the drying time needed to cure the inks. Moreover, the environmental impact of radiation drying is less when compared to the hot-air drying process. The main types of radiation drying are UV, LED- UV, Electron beam and microwave drying.

The UV dryers consist of a beam source and reflector. The UV light transforms the liquid ink present in the printed substrate into a solid form through a photo-polymerization process. For UV drying, the inks must be of a special type that reacts to UV radiation. The ink curing can be completed within a fraction of a second with UV drying, thereby helping achieve high production speed. Since there is no evaporation of solvents in UV curing inks, it is a better solution for environmentally friendly drying without VOC emissions to the atmosphere. In addition, the print quality and print stability of UV drying are high. However, high energy consumption, ozone emissions, and huge capital investment are the drawbacks of conventional UV drying. LED-UV drying is an innovative system that uses diodes to convert electrical energy to light, and the UV radiation then converts the liquid ink film to solid by polymerisation. Compared to conventional UV systems, LED-UV consumes less energy and has a lower rate of emissions, which helps achieve sustainable goals [10].

Electron beam drying is also an alternative to the traditional drying process. In electron beam drying, the high-energy electrons are accelerated towards the printed substrate to cure the inks. The chances of overheating the substrate are comparatively low, thereby saving energy for the cooling process.

A study conducted on the printing and publishing industries by Margolis et al. [11] suggests that by replacing natural gas hot air drying with UV and Electron beam drying, energy consumption can be reduced by 50%. Higher capital costs and the need for special types of inks in UV and Electron beam drying are the main factors that limit their application in flexographic industries.

Microwave drying is a non-ionizing radiation drying process where the molecule in the heated medium becomes polarised with positive and negative charges by a microwave electromagnetic field. Several tests were conducted by Marios et al. [12] to identify the drying rate and energy consumption of different types of radiation drying and evaporative drying on flexographic water-based inks. Results showed that microwave drying consumes less energy and drying time compared to other drying processes, such as infrared and hot-air drying.

Implementing energy-efficient and low-emission drying technologies in the flexographic printing process is essential. It ensures both economic and environmental sustainability. Future research should focus on optimising drying parameters and exploring sustainable ink formulations to further enhance the efficiency and sustainability of flexographic printing processes.

1.4 Lean techniques in flexographic printing

Manufacturing processes use lean methodologies to improve energy efficiency and productivity. These methods also help eliminate waste and reduce the overall cost of production. The value stream mapping, 5 why analysis, SMED, and Kaizen methods can be combined as a lean approach to enhance energy and process efficiency. The first step in the lean method is the proper identification of problematic areas where improvements are needed. After that, the root cause of this problem can be investigated with a 5-why analysis. Later, improvements can be developed to achieve better overall equipment effectiveness using the Kaizen approach. Finally, the proposed idea is implemented in the existing process for better efficiency.

A study conducted by Zahoor et al. [13] improved the overall equipment efficiency of a flexographic machine by reducing the breakdown time with the help of total productive maintenance measures. 5-whys analysis techniques were implemented to analyse the root cause of the breakdown time and thereby improved the overall efficiency from 34% to 40.2%. Similar to the work of [13], the Overall Equipment Effectiveness of a flexographic printing machine is improved by 24% with the implementation of visual stream mapping, 5- why root cause analysis and kaizen lean approach [14].

In the manufacturing of flexographic printed substrates, the idle time needed for job setting, job changeover, job

waiting, and optimisation of process parameters is normally very high. Even though the machine does not produce any printed material during idle time, it consumes a considerable amount of energy. This is because the pumps, motors, and other mechanical and electrical devices are still working and consume energy during idle time. A study was conducted by Ivander et al. [15] to increase production efficiency by reducing the setup time in a flexographic machine with the Single Minute Exchange of Dies (SMED) and the Internet of Things method. The result shows that the implementation of the SMED method reduced the set-up time by 9.7 minutes. The study also proposes implementing the Internet of Things in the machine to reduce setup time in the future. Another study conducted by Zaher et al. [16] on flexographic printing machines to improve energy efficiency by applying Lean principles such as 5 why analysis and kaizen approach during production job. The study found that by reducing the idle time of Miraflex and F&K flexographic machines by 30%, energy savings of 34.198% and 38.635% can be achieved respectively per meter.

1.5 Artificial intelligence and machine learning

Artificial intelligence and machine learning techniques are used in industries that optimise energy consumption. A regression model using Python was developed by Zaher et al. [16] to predict the energy consumption of flexographic machines for optimising the scheduling of jobs. The input parameters used in the model were machine speed, substrate density, total run time of the machine, working time, idle time, and produced meter. A limitation of the work is that the main process parameters that influence the energy demand, such as air speed and temperature for the drying process, were not considered in the energy prediction model. Menezes et al. [17] developed a linear programming mathematical model for printing industries to optimise energy consumption. The main goals of the work were to reduce the electrical energy consumption of the machine and to minimise the machine's production time by implementing optimisation techniques to assist with production planning, scheduling, and control in the printing industry.

1.6 Limitations of the existing works

The main limitation of the existing research works is the lack of a well-defined systematic method to identify the possible scope of energy savings opportunities and sustainable solutions in flexographic printing machines at a sub-unit process level. **Fig.5.** shows the less explored areas in flexographic printing that need to be investigated in detail. Even though flexographic printing machine uses many energy-consuming devices such as motor drives, dryer units, pumps, and ventilation fans and releases direct emissions, heat, and wastes into the atmosphere, the lack of a detailed energy breakdown analysis on the flexographic printing machine and their corresponding processes is still a research problem to solve. Moreover, less research was carried out on the auxiliary units that support the manufacturing of the flexographic printing process.

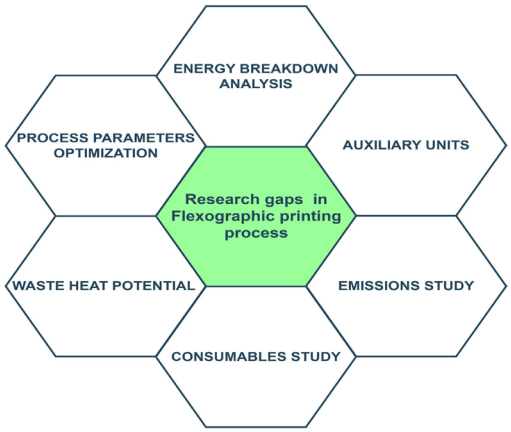

Fig. 5. Research gaps in the flexographic printing process.

Compressed air is generally used for a variety of purposes, and industrial chillers are used in flexographic printing. However, no investigations were carried out to quantify the energy demand of chiller and compressed air units to explore the possible scope of energy savings. Since flexographic printing can be applied to a wide range of applications and different types of jobs, optimising the main process parameters for different job types for energy savings is still an unanswered research question.

The know-how energy efficiency solutions in other industrial processes can also be integrated into flexographic printing. Still, there is a knowledge gap in identifying the right processes or areas to implement innovative solutions for energy savings. Therefore, an in-depth analysis of the flexographic printing machine at a single process sub-unit level, which includes the auxiliary support units, is needed to identify the main energy and resource-consuming hot spots and their corresponding emissions for implementing innovative and sustainable solutions in the relevant sections.

2. Materials and Methods

To address the research gap, a flexographic printing machine, Onyx Race, which has a maximum printing speed of 600 m/min and uses natural gas burners for hot air drying, is analysed in the case study. The machine has a Central impression printing unit consisting of eight colour stations. It is capable of printing on a wide variety of substrates, such as plastics, paper, and aluminium, with the flexibility to use water-based and solvent-based inks.

A detailed data collection was conducted to gather information on relevant sub-units, including auxiliary units in the machine. Semi-structured interviews were conducted with product innovation engineers, technicians, and machine operators in the manufacturing industry to identify the various processes involved in the flexographic machine at different phases of production.

The web passes from the unwinder undergoes a corona treatment (infeed unit) before passing to the printing unit to improve the surface energy of the substrate if the material to be printed is plastic. The corona treatment unit

releases ozone gas, which is removed from the machine with an exhaust fan. Apart from the main drying tunnel, the machine has separate drying boxes for each colour unit in the flexographic printing group section, except for the last colour unit. Two separate gas burners with ventilation fan units are used for hot air drying in the printing group section and drying tunnel. An air-cooled chiller is used in the machine with an on-off control for the compressor. In addition to cooling the web passes through the outfeed roller, chilled water is also used to cool the motors. The Central impression drum is also maintained at a particular set point temperature with the thermoregulation unit in the chillers. When the printing job needs to be changed, the washing and cleaning of the anilox, cliché, and entire printing units are done with either solvents or water, depending on the type of ink used. The washing and cleaning process is the main source of liquid emissions in flexographic printing. The compressed air is used in the machine to pump inks and solvents, anilox and cliché change, nip pump, etc.

A life cycle-oriented in-depth approach is proposed for the use phase (operating stage) of the flexographic printing machine, which includes an energy, consumables, and emissions study at a sub-unit process level. [18]. The study excludes the rest of the life cycle phases of the machine, such as material processing, production, and disposal. Also, the post-treatment process involved in removing the VOC solvent content in exhaust air, leaving the drying sections is excluded from the scope of this study. The main goal of the Life cycle-oriented analysis in a flexographic printing machine is to identify the environmental impact and emissions released from each process as well as the energy and resource-consuming sub-units in the manufacturing of flexographic printed substrates.

The input consumables and the corresponding emissions from the machine during each process were identified. The system boundaries of the machine were defined with the input and output flows [19]. An understanding of the main process parameters that influence the energy consumption of the machine was identified with a preliminary test campaign. To identify the unknown flows in each process of the LCA, a detailed measurement test plan is proposed for the flexographic machine through a careful examination of the machine and its sub-units.

In the main test campaign, different varieties of substrate materials can be printed at various production speeds with different print widths, ink types, and ink coverage to explore the variations in energy demand and corresponding emissions in each case. The results obtained from the measurements campaign can be analysed more deeply to implement innovative solutions that minimise the energy demand and environmental impact of flexographic printing. A flow diagram illustrating the systematic approach used in this study is shown in Fig. 6.

3. Results and Discussion

The system boundaries have been defined, and the input and output flows of the main relevant processes and subunits in the flexographic machine are shown in **Fig.7**. The functional unit selected in the analysis is the production of printed substrate per tonne. The main process parameters that influence the power demand are hot-air temperature, ventilation fan speed, machine production speed, and material tension.

3.1 Energy Breakdown Analysis

A detailed measurement test plan is presented in this section to identify the electrical and thermal energy demand, both as a whole and at a sub-unit level, for different production phases of the machine. Since energy demand is calculated by multiplying power consumption with operational time, a power and time study is being conducted to perform the energy analysis.

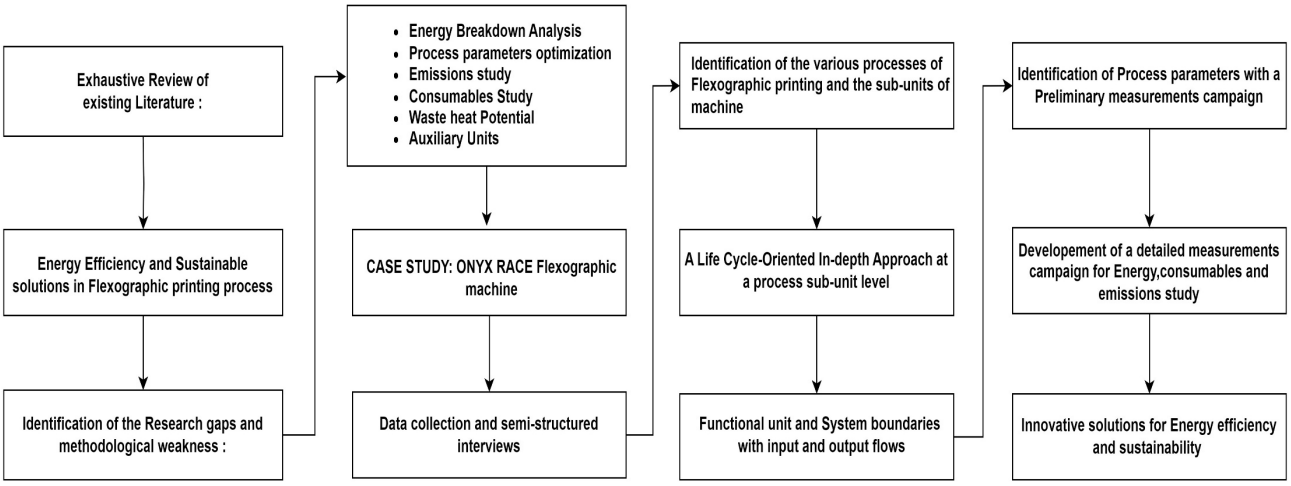

Fig.6. Flow diagram of a systematic approach used to identify the energy savings and sustainable solutions in the flexographic process

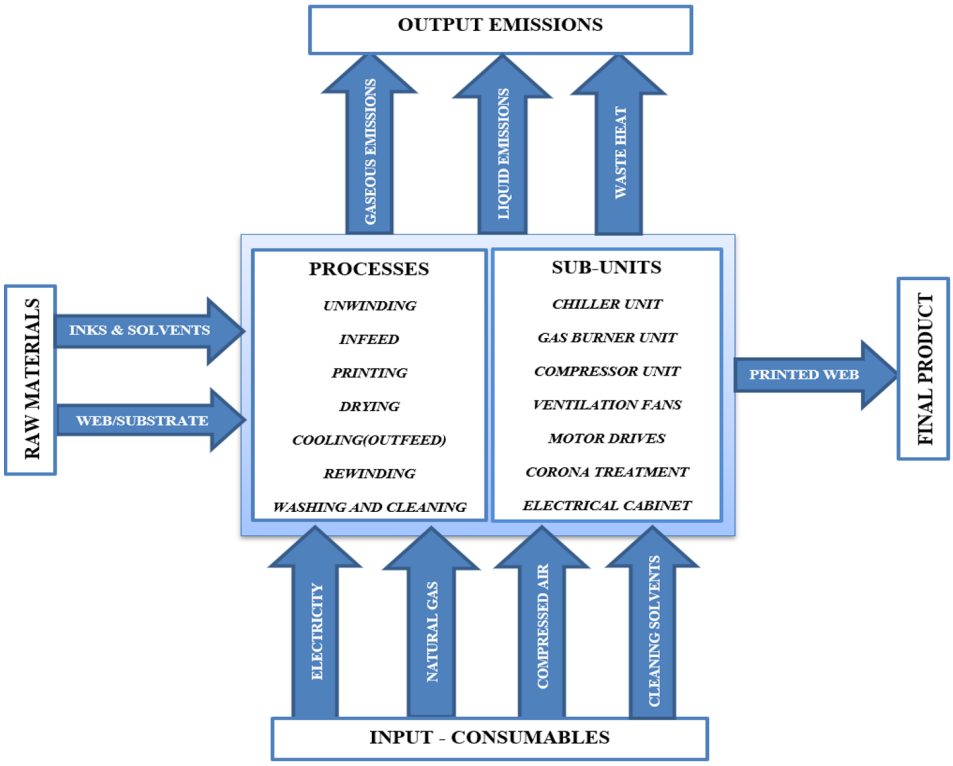

Fig. 7. LCA: System boundaries for the flexographic printing machine with input and output flows

Power and time study

The total electrical power consumption of the Onyx Race flexographic machine, along with the power demand of relevant sub-units, such as chiller, motor drives, and ventilation fans, was measured simultaneously using power analysers during production. The electrical power consumption of the ventilation fan motors used in the inlet and outlet sections of drying units was measured separately. The thermal power demand of the two gas burners in the machine for the drying process is also being monitored and analysed in detail.

The measurements of the chiller unit include not only the total electrical power demand of the chiller but also the compressor power, heater power, pump power, and heat load (measurements by flow rate and temperature sensors) removed by cooling processes and thermoregulation unit.

The influence of the main process parameters on the total power demand of the machine, such as drying air temperature, ventilation fans speed, and material tension, is being investigated for several types of jobs (different ink coverage, ink type, substrate material, print width) at various production speeds.

The different production phases of the machine, such as the start-up mode, job setting mode, productive mode, job-changeover mode, and shutdown mode, and their corresponding time, were investigated in the time study. Thus, the energy demand needed for each production phase of the flexographic machine as a total and at the subunit level can be identified with the power and time study. Once the complete measurements are done, special focus can be given to the main consuming processes and sub-units of the machine for the possible scope of energy savings with innovative solutions.

3.2 Consumables study.

In the consumables study, the consumption of raw materials used in the flexographic printing process such as compressed air, natural gas, substrate material, inks, and solvents are being measured during production. The natural gas consumed by the gas burners, which heat the inlet air to the required drying temperature, is being measured using gas flow meters compensated to standard temperature and pressure.

The compressed air consumption in the machine for various purposes, such as pumping of inks and solvents, anilox and sleeve change, etc., is being measured (flow rate and pressure) at a sub-unit level with flow meters. The consumption of solvents or water used for the washing and cleaning process in the machine is also being monitored with flowmeters.

3.3 Emission study

The waste heat, liquid and gaseous emissions rejected from the machine during the production phases of the printed substrate are being mainly investigated as the main parameters in the emissions study. Since the exhaust air leaving the drying section of the machine releases

waste heat and direct emissions, such as VOC and CO2, to the atmosphere, special attention must be given to this section.

The main unknowns in the energy and mass flow balance equations in the relevant sections of the drying unit are being determined by experimental measurements.

The waste heat lost from the drying units through exhaust air can be calculated by the equation:

$$Q = V \times \rho \times C \times (T_2 - T_1) \quad (1)$$

Where Q is the heat energy losses, V is the volumetric flow rate, ρ is the density of air, C is the specific heat capacity of air, T_2 is the temperature of exhaust air, and T_1 is the temperature of inlet fresh air.

The waste heat rejected from the chiller unit ($Q_{chiller}$) can be calculated by measuring the heat removed by cooling processes (Q_{load}) and the electrical power consumption of the compressor ($W_{compressor}$).

$$Q_{chiller} = Q_{load} + W_{compressor} \quad (2)$$

Additionally, the sensible heat transferred to the substrate material from the drying process is being monitored using infrared sensors.

Finally, the ozone gases removed from the corona treatment unit can also be quantified in the study.

3.4 Future scope of energy savings in Flexographic printing

Based on the observations from a preliminary analysis of the machine, the main areas for energy efficiency improvements identified are waste heat rejected from the machine, process parameters optimisation, implementation of AI and machine learning techniques, energy efficiency measures for chiller, compressed air, ventilation fans, and motor drives unit. Innovative solutions can be implemented for each of the sections for long-term energy savings and sustainability. Among the different areas for improvisations, the thermal energy demand for the drying process and waste heat lost from the subunits of the machine are expected to be the main hot spots where efficient solutions can be implemented with a top priority.

The waste heat lost from the drying process through exhaust air could be recovered by heat recovery techniques to preheat the inlet air for energy savings [20]. It reduces the thermal energy demand and natural gas consumption of the drying process with a considerable reduction in direct emissions. Moreover, the sensible heat lost from the drying section to the printed material due to overheating (dry-out point) can be monitored with infrared sensors, thereby optimising the process parameters in the drying unit for further energy savings. At higher production speed, the time needed for drying (ink curing) the printed substrate is a challenge in flexographic printing and drying quality must be guaranteed with the corresponding production speed to ensure product quality.

With in-line measurement devices, the drying quality of the substrate at higher production speeds can be determined quickly, and the process optimisation could be done by quick feedback and a faster response system that reduces downtime.

The main process parameters could also be optimised for energy savings based on different types of job conditions, such as substrate material, ink coverage, print width, and production speed, by implementing AI and machine learning techniques. The possible scope of recovering the waste heat lost from the condenser of an air-cooled chiller to use it for other processes could be investigated in the study. The scope of integrating the free cooling option for the chiller unit during colder months of the year could also be a possibility for energy savings. The on-off control of the compressor increases energy demand by causing frequent cycling between on and off states, which leads to inefficient energy use. During startup, the compressor requires more energy to reach its operating capacity, and the constant cycling prevents the system from maintaining a steady, efficient operation, resulting in higher overall energy consumption. Replacing the on-off controlled compressor of the chiller with a Variable Speed Drive-controlled compressor can be useful for energy savings at part-load conditions [21].

Compressed air systems in industries are usually not an efficient way of energy usage. From the total energy demand of the compressed air unit, only 15-25% could be utilised as useful work, and the rest is lost as waste heat [22]. Replacing the compressed air sub-units with energy-efficient alternatives such as electrical devices could be a solution for energy savings in flexographic machines. If some of the compressed air sub-units cannot be replaced due to easiness, flexibility, and safety in operation, the waste heat rejected from the compressed air unit could also be investigated to explore the possible scope of recovery for other processes. Energy savings can be made possible by finding the lowest operating air pressure for the compressed air sub-units without losing the end-service quality. A proper monitoring system can be installed to eliminate the leaks, and de-centralization of the compressed air unit from the industry to the machine level could also save energy.

The electric motors used in industrial machines are generally oversized for safety reasons and operate at lower load conditions. As motor efficiency varies with load, appropriate motors can be selected for the machine at their most efficient load condition for energy savings. Replacing the impeller of the ventilation fans with efficient ones or redesigning the ducts in the machine could also be investigated for further energy savings [23]. Innovative nozzles could be used in the drying unit for efficient drying and energy savings. Finally, using environmentally friendly inks, recycling the waste solvents and substrate for reuse options, and upgrading the conventional hot air-drying systems with innovative drying technologies such as

LED-UV and Electron beam drying could not only save energy but also largely reduce the environmental impact to a greater extent.

4. Conclusion

The study identified the existing research gaps in the flexographic printing process, followed by a literature review and aimed to provide a proper methodology for identifying the energy saving opportunities and sustainability solutions in flexographic printing. A case study on a flexographic printing machine was considered to explore future research possibilities. A life cycle-oriented in-depth analysis is presented for the use phase (production phase) of the machine, which includes the energy, emissions, and consumables study at a sub-unit process level of the machine by identifying all the input and output flows. The main parameters that influence the energy consumption of the machine were identified to explore the scope of optimisation of process parameters for energy savings.

A detailed measurement test plan is proposed at a sub-unit level to identify the unknown flows through the machine in the Life cycle analysis. The waste heat rejected from various processes in the flexographic machine is the main hot spot where improvements can be made for energy savings. Heat recovery techniques can be implemented for the drying unit and chiller to recover energy lost to the atmosphere and utilise it efficiently. Heat recovery techniques not only reduce the natural gas consumption (thermal demand) needed to heat the air during the drying process but also minimise the corresponding direct emissions from it. Process parameters can be optimised with in-line measurement sensors to improve the quality of the printed substrate and save energy. Implementing AI and machine learning techniques in flexographic printing could also save energy by optimising process parameters for different types of job conditions. Installing variable speed drive-controlled compressors for the chiller, replacing the oversized motors and inefficient pumps with efficient ones, changing impeller fan configurations, and upgrading the nozzles of the drying unit could also save energy, improve machine efficiency, and reduce carbon footprint.

The feasibility of the proposed ideas can be validated through the results of the measurement test campaign. After that, feasible solutions can be developed and implemented in the relevant sections of the flexographic printing machine for long-term energy savings and production efficiency. Thus, the packaging print and conversion industries can reduce their carbon footprint and achieve sustainability goals in the manufacturing of flexographic printed substrates, along with economic benefits.

5. References

[1] “Industry - Energy System - IEA.” Accessed: Jul. 31, 2024. [Online]. Available: https://www.iea.org/energy-system/industry

[2] “Flexographic Printing Market Share & Size Report, 2023 – 2032.” Accessed: Jul. 31,2024. [Online]. Available: https://www.gminsights.com/industry-analysis/flexographic-printing-market

[3] “File: Flexographic printing diagram.svg - Wikimedia Commons.” Accessed: Aug. 13,2024. [Online].Available: https://commons.wikimedia.org/wiki/File:Flexographic_printing_diagram.svg

[4] X. Jingxiang, L. Jinyao, L. Haichao, Z. Mingming, and C. Jifei, “Research Progress on Water-based Ink Drying Technology,” in IOP Conference Series: Materials Science and Engineering, Institute of Physics Publishing, Jun. 2019. doi: 10.1088/1757-899X/565/1/012017.

[5] H. Hardisty, “An investigation into the drying of thin films of ink, using infra-red dryness measurement,” Ph.D thesis, University of Bath, 1980.

[6] A. Avcõ, M. Can, and A. B. Etemogae, “A theoretical approach to the drying process of thin film layers,” 2001. [Online]. Available: www.elsevier.com/locate/apthermeng

[7] B. Turkan, A. B. Etemoglu, and M. Can, “An investigation into evaporative ink drying process on forced convective heat and mass transfer under impinging air jets,” Heat and Mass Transfer/Waerme- und Stoffuebertragung, vol. 55, no. 5, pp. 1359–1369, May 2019, doi: 10.1007/s00231-018-2515-z.

[8] P. Viluksela, Environmental sustainability in the Finnish printing and publishing industry. 2008.

[9] I. Kliopova-Galickaja and D. Kliaugaite, “VOC emission reduction and energy efficiency in the flexible packaging printing processes: analysis and implementation,” Clean Technol Environ Policy, vol. 20, no. 8, pp. 1805–1818, Oct. 2018, doi: 10.1007/s10098-018-1571-x.

[10] I. Bolanča Mirković, G. Medek, and Z. Bolanča, “Ecologically sustainable printing: Aspects of printing materials,” Tehnicki Vjesnik, vol. 26, no. 3, pp. 662–667, 2019, doi: 10.17559/TV-20180620181128.

[11] N. G. Margolis and J. L. Pellegrino, “ENERGY EFFICIENCY IN THE PRINTING AND PUBLISHING INDUSTRIES.”

[12] M. Tsigonias et al., “Using microwave drying systems in the Graphic Arts. Modern solutions for environmental industrial applications. Using microwave drying systems in the Graphic Arts. Modern solutions for environmental industrial applications,” 2010, doi: 10.13140/2.1.4214.9449.

[13] S. Zahoor, A. Shehzad, N. A. Mufti, Z. Zahoor, and U. Saeed, “Overall equipment efficiency of Flexographic Printing process: A case study,” in IOP Conference Series: Materials Science and Engineering, Institute of Physics Publishing, Dec. 2017. doi: 10.1088/1757-899X/272/1/012015.

[14] S. Zahoor, W. Abdul-Kader, H. Ijaz, A. Khan, Z. Saeed, and S. Muzaffar, “A Combined VSM and Kaizen Approach for Sustainable Continuous Process Improvement,” International Journal of Industrial Engineering and Operations Management, vol. 01, no. 02, Dec. 2019, doi: 10.46254/j.ieom.20190203.

[15] Ivander, T. H. S. Rimo, and F. A. O. Reynaldi, “Setup time reduction in flexo machine with SMED and internet of thing method,” in IOP Conference Series: Earth and Environmental Science, IOP Publishing Ltd, Aug. 2021. doi: 10.1088/1755-1315/794/1/012089.

[16] Z. Abusaq et al., “Improving Energy Performance in Flexographic Printing Process through Lean and AI Techniques: A Case Study,” Energies (Basel), vol. 16, no. 4, Feb. 2023, doi: 10.3390/en16041972.

[17] L. F. de Menezes, A. R. Balbo, A. C. Cherri, S. C. Poltroniere, C.

T. L. da Silva Ghidini, and E. M. Soler, "Energy consumption optimization in a printing company," Gestao e Producao, vol. 31, 2024, doi: 10.1590/1806-9649-2024v31e1723.

[18] K. Kellens, W. Dewulf, M. Overcash, M. Z. Hauschild, and J. R. Duflou, "Methodology for systematic analysis and improvement of manufacturing unit process life-cycle inventory (UPLCI)-CO2PE! initiative (cooperative effort on process emissions in manufacturing). Part 1: Methodology description,"International Journal of Life Cycle Assessment, vol. 17, no. 1, pp. 69–78, Jan. 2012, doi: 10.1007/s11367-011-0340-4.

[19] K. Kellens, W. Dewulf, M. Overcash, M. Z. Hauschild, and J. R. Duflou, "Methodology for systematic analysis and improvement of manufacturing unit process life cycle inventory (UPLCI) CO2PE! Initiative (cooperative effort on process emissions in manufacturing). Part 2: Case studies," International Journal of Life Cycle Assessment, vol. 17, no. 2, pp. 242–251, Feb. 2012, doi: 10.1007/s11367-011-0352-0.

[20] H. Jouhara, N. Khordehgah, S. Almahmoud, B. Delpech, A. Chauhan, and S. A. Tassou, "Waste heat recovery technologies and applications," Jun. 01, 2018, Elsevier Ltd. doi: 10.1016/j.tsep.2018.04.017.

[21] P. Olszewski, "Experimental analysis of ON/OFF and variable speed drive controlled industrial chiller towards energy-efficient operation," Appl Energy, vol. 309, Mar. 2022, doi: 10.1016/j.apenergy.2021.118440.

[22] R. Saidur, N. A. Rahim, and M. Hasanuzzaman, "A review on compressed-air energy use and energy savings," May 2010. doi: 10.1016/j.rser.2009.11.013.

[23] V. R. Babu, T. Maity, and H. Prasad, "Energy saving techniques for ventilation fans used in underground coal mines—A survey," Journal of Mining Science, vol. 51, no. 5, pp. 1001–1008, Sep. 2015, doi: 10.1134/S1062739115050198.

Yuxuan Zhang[1], Xiaoqiang Zhai[2], Zihao Zhou[1], Xiaolin Wang[1]

Numerical Exploration of Flow and Thermal Performance in Packed-Bed Cold Storage Enhanced by Structured PCM Capsule Layouts

[1]Research School of Engineering, The Australian National University, Canberra, ACT 2601, Australia
[2]Institute of Refrigeration and Cryogenics, Shanghai Jiao Tong University, Shanghai, 200240, China

Abstract

Understanding how the layout of phase change material (PCM) capsules influences the performance of cold thermal storage systems advances designs that maximize energy storage capacity, minimize energy losses, and improve the overall sustainability of cooling applications. Based on the closest packing principle of the crystal structure, two layouts of the spheres in cylindrical packed beds, i.e. face-centered cubic (FCC) and hexagonal closest packed (HCP), are proposed in this paper. The flow and heat transfer performance of these two packing layouts is numerically investigated. Firstly, efforts are made to figure out the thermal-hydraulic mechanisms of different packing layouts under laminar steady flows. They are compared with the conventional aligned dense layer (ADL) packing with Reynolds number in the range of 1–200. The results show that, compared with the ADL packing, the theoretical PCM packing density for HCP and FCC layouts is raised by 22.5%, thus considerably saving the space required of the packed bed. FCC packing layout achieves the best flow and thermal performance, followed by HCP packing. Secondly, PCM transient thermal performance in the whole packed beds with the three packing layouts are studied during the charging process. It is found that the FCC bed has the highest heat transfer capability at a constant flow rate of 100 L/h, with a shorter charging time by 21.4% compared to that of the conventional ADL packing.

***Keywords**: phase change material; packed-bed cold storage; energy storage density; charging time; pressure loss*

Nomenclature

A	surface area (m^2)
c	specific heat capacity ($J \cdot kg^{-1} \cdot K^{-1}$)
d	diameter (m)
d_h	pore-scale hydraulic diameter (m)
D	diameter of packed unit (m)
h	sensible heat of phase change material ($kJ \cdot kg^{-1}$)
H	total enthalpy of phase change material ($kJ \cdot kg^{-1}$)
ΔH	latent heat of phase change ($kJ \cdot kg^{-1}$)
JF	overall thermal performance factor
k	thermal conductivity ($W \cdot m^{-1} \cdot K^{-1}$)
L	length (m)
n	number of data
Re	Reynolds number
Nu_{aver}	surface average Nusselt number
p	pressure (Pa)

q_s heat flux of the active ball ($W \cdot m^{-2}$)
t time (s)
T temperature (ºC)
$\overline{T}_f$ volume average temperature of HTF (ºC)
$\overline{T}_s$ surface average temperature of the active ball (ºC)
T_r temperature at the time of τ by simulation (ºC)
T_r' temperature at the time of τ by experiment (ºC)
u velocity ($m \cdot s^{-1}$)
V volume (m^3)
x distance (m)

Greek symbols

ρ density ($kg \cdot m^{-3}$)
φ porosity
τ time step (s)

Subscripts

f heat transfer fluid
i i-th direction
in inlet
ini initial time
p phase change material
s surface of the spherical capsule

Abbreviations

ADL aligned dense layer
BCC body-centred cubic
FCC face-centred cubic
HCP hexagonal closest packed
HTF heat transfer fluid
MAPE Mean Absolute Percentage Error
PCM phase change material
SC simple cubic
TES thermal energy storage
RBC red blood cell
RMSE root mean square error

1. Introduction

As environmental problems are getting increasingly severe, the utilization of renewable energy resources becomes a hot topic of common concern (Gielen et al., 2019). However, most of the renewable energy is intermittent and periodical by nature, which makes it difficult to be harnessed in real applications if there were no appropriate measures (Helm & Mier, 2019). Under this context, thermal energy storage (TES), which stores thermal energy to bridge the mismatch between energy supply and demand, is widely applied in various areas, such as solar thermal systems, waste heat recovery and air conditioning systems (Fleuchaus et al., 2018). Compared with sensible TES, latent thermal energy storage is more favorable due to its high energy storage density and isothermal behavior during the phase change process (Diao et al., 2019).

With the development of phase change materials (PCMs), a number of studies have been conducted for cold storage applications. Fin tube phase change cold storage has been widely studied with the annular fin pitch and the number and height of fins as the key structural metrics for optimization (Zhai et al., 2015). With the advancement of PCM encapsulations, packed-bed cold storage has attracted extensive interest for its high storage density and large heat transfer area (Bindra et al., 2013; Chen et al., 2019). There are four widely studied areas regarding packed-bed cold storage, of which one is the formation of cold storage units. A cascaded packed-bed PCM cold storage unit was numerically studied by Cheng et al. (Cheng & Zhai, 2018a) and compared with a single-stage cold storage unit. The results showed that a 24-stage cold storage with a phase change temperature difference between the highest and lowest stage of 6 °C was optimal with a 15.1% reduction in charging time compared to a single-stage one. Although the cooling capacity and exergy stored in cascaded cold storage were less than those in a single-stage one, the charging rate and exergy efficiency were dramatically increased (Cheng & Zhai, 2018b). It was also found by Li et al. (B. Li et al., 2019), through a one-dimensional transient model of a cascaded packed-bed cold storage, that the multiple stages made the phase change process faster and more uniform. Second, the internal structure of PCM capsules has been optimized. Jia et al. (Jia et al., 2019) carried out an experimental and numerical study on a spherical PCM capsule with circular pin-fins, in terms of the internal temperature, liquid fraction and charging rate of capsules with various pin-fin configurations. It was found that the charging rate was improved dramatically by adding fins, and the charging time was decreased by >50% in capsule with six fins compared to that without fins. Third, novel geometric structures of PCM capsules have been proposed. An innovative red blood cell (RBC) shaped PCM capsule was studied by Cheng et al. through experiment and simulation (Cheng & Zhai, 2017). Its thermal performance was compared to that of various deformation structures, e.g. cylinder, drum, ring and sphere. The results revealed that the RBC-shaped capsule had the best thermal performance.

In the following work (Cheng et al., 2020), forced convection of external flows over an RBC-shaped PCM capsule was numerically studied in a steady-state laminar flow region. It was found that the drag coefficient of the capsule decreased with the increase of Reynolds number. 0° attack angle was recommended for the RBC-shaped capsule for its low drag force and high Nusselt number. The last aspect of packed-bed cold storage studies is the capsule layout and configuration in the packed bed to improve the fluid flow and thermal performances in the packed beds. Halkarni et al. (Halkarni et al., 2017) estimated the local

wall heat transfer coefficient by infrared (IR) thermography in the packed beds randomly filled with uniformly sized spheres. Lee and Chung (Lee & Chung, 2019) experimentally investigated the forced convective heat transfer across heated spheres in packed beds. The results indicated that the Nusselt number decreased as the ratio of bed height to sphere diameter increased due to the axial dispersion. Zenner et al. (Zenner et al., 2019) presented a new robust experimental setup and demonstrated that the size of the cylinder and the diameter of the inner holes were central to generalizing the thermal performance and the pressure drop in the packed bed. Yeboah and Darkwa (Yeboah & Darkwa, 2019) compared a Z-annular flow configuration and conventional packed beds of the same dimension. It was concluded that the Z-annular flow configuration had the potential to enhance the heat transfer and storage capacity. Guo et al. (Guo et al., 2019) constructed a free channel, flow guiding conduit (FGC), in the center of a packed bed using highly fluid-penetrable material, thus promoting flow in the lateral direction with Venturi effect. According to the results, the capsule layout plays a significant role in the hydrodynamic and heat transfer performance in real applications.

To date, randomly packed beds have witnessed substantial efforts in the literature to improve their flow and heat transfer performances. Halkarni et al. (Halkarni et al., 2016) used a transient technique to measure volumetric heat transfer coefficient in randomly packed beds with uniformly sized spheres. There was an increase in the volumetric heat transfer coefficient with the increase in Reynolds number. Das et al. (Das et al., 2017) presented a fully resolved direct numerical model of a slender random packed-bed reactor.

Correlations of the pressure drop and the overall heat transfer coefficient were proposed. It was seen that the pressure drops in randomly packed beds were reduced largely and the corresponding heat transfer performance was improved by the superior configurations. Guo and Dai (Guo & Dai, 2010) presented a fully resolved direct numerical model of a slender randomly packed bed and found the fully resolved accurate numerical simulations helped toelucidate detailed pore-scale flow and heat transfer features. Calis et al. (Calis et al., 2001) set up a randomly packed pebble bed test facility and proposed a new correlation to predict the pressure drop and convective heat transfer characteristics in the bed. However, inevitable shortcomings were noticed in random packing systems as the pressure drop was typically far higher than other packing forms. Moreover, it is evident that the flow and heat transfer distribution is inhomogeneous in such packed beds, and it is difficult to predict the location of the hotspot (Sobes et al., 2011).

To address the above issues, structured packed beds are proposed instead of traditional randomly packed beds. Calis et al. (Calis et al., 2001) and Romkes et al. (Romkes et al., 2003) compared the thermal-hydraulic performance of five packing forms of composite structured packed beds both numerically and experimentally. The results revealed that the pressure loss was reduced remarkably and the heat transfer characteristics were affected greatly by means of composite structured packing. Qian et al. (Qian et al., 2019) proposed a kind of grille-sphere composite packed bed and found that the pressure drop was decreased and the radial heat transfer performance was increased compared with a randomly packed bed. Guo et al. (Guo et al., 2017; Guo et al., 2019) proposed a kind of slender packed beds with novel packing layouts, where particles in contact with the wall tended to form a highly ordered ring structure, thus rendering the pressure drop decreased and heat transfer efficiency enhanced to some extent. Tian et al. (Tian et al., 2018) experimentally explored fluid flow and heat transfer characteristics of power-law fluid in wall-bounded three-dimensional structured packed beds of spheres. The relationship between the pressure drop and flow velocity was verified by modified Ergun type equations. Guo et al. (Guo et al. , 2019) studied the effects of the confining wall on particle-to-fluid convective heat transfer and pressure drop, and found two different flow distributions in the packed beds, i.e. the wall-channeling type and the regular-packing-dominating type. Toghraie et al. (Toghraie et al., 2018) investigated wall effects on the cross and axial flow and heat transfer of particles in a packed bed and found that heat transfer improved as the particle moves closer to the wall.

To further analyze effects on thermal-hydraulic performance affected by capsule layout, Hu et al. (Hu et al., 2019; Hu et al., 2018) and Wang et al. (Wang et al., 2018) classified the packing configuration into three types, including simple cubic (SC), body-centered cubic (BCC) and face-centered cubic (FCC) ones. The simulation and experimental work on the flow and heat transfer characteristics were extensively carried out in the packed beds with internal spherical particles and external rectangular tanks. It was found that these novel structures had a remarkable capability for decreasing pressure loss and enhancing heat transfer efficiency, echoed by Guo et al. (Guo et al., 2019) and Chen et al. (Chen et al., 2017).

Despite the reduced pressure loss of loose packed-bed layouts, it is noted that these packed beds are featured by large volume size and high manufacturing cost of the tank due to their high porosity and low energy storage density. It may limit the implementation of PCM packed beds (T. Li et al., 2019). On the other hand, to the best of our knowledge, the existing investigation on packing structures mainly focuses on rectangular containers, while the arrangements of spheres in cylindrical ones, which are more suitable for PCM cold storage, are rarely mentioned in the literature. Compared to rectangular configurations, cylindrical packed beds offer distinct advantages for PCM cold storage, including inherent structural robustness to withstand thermal and mechanical stresses, radial symmetry for uniform heat distribution, and compactness that minimizes surface-area-to-volume ratios and thermal losses. Their geometry aligns naturally with industrial standards for pressurized systems, enabling seamless integration into real-world applications such as HVAC and thermal energy storage units. Furthermore, the concentric arrangement of capsules in cylindrical beds enhances packing density and flow uniformity, addressing critical challenges in scalability and thermal performance. To overcome the issues of large packed bed volume, this study was inspired by the arrangement of atoms or ions in metal and ionic lattices, which can be geometrically

regarded as packing of uniform spheres, where crystals tend to lie in the most stabilized or lowest internal energy state (Grosso & Parravicini, 2013).

From this perspective, spheres get as close to each other as possible, thus occupying the minimum space. Based on the closest packing principle of crystal structures, two novel packing configurations of spherical capsules, i.e. FCC (same as aforementioned) and hexagonal closest packed (HCP), are proposed in the present study for cylindrically packed-bed PCM cold storage. Through a numerical study using ANSYS Fluent 18.0, the hydrodynamic and heat transfer performances of these two packed forms are comprehensively compared with that of the conventional ADL packing layout. First, the transient thermal performances and pressure loss in the whole packed beds with different capsule layouts were studied during PCM solidification, to examine the advantages of diverse packing configurations in cold storage applications. In addition, the power consumption together with a self-developed new metric, the normalized charging efficiency factor, were employed to evaluate the three packing configurations, which provided important advancement of knowledge to future studies.

2. Numerical methods

2.1. Physical model of packed-bed cold storage tank

As illustrated in **Fig. 1** (a), the 171 spherical PCM capsules with an identical inner radius of 20 mm, with a shell thickness of 1 mm, were stacked sequentially in a conventional cylindrical packed bed (ADL) with an inner diameter of 220 mm (including gaps between capsules) and a rated cold storage capacity identical to 576.3 kJ. The capsules were divided into nine layers with 19 capsules in each layer. Water, as the heat transfer fluid (HTF), flew into the packed-bed tank from the bottom to the top during the charging process as a laminar steady flow. Based on this configuration, two typical dense packing configurations of the cold storage tank, i.e. the HCP and FCC layouts, were developed as schematically depicted in **Fig. 1** (b) and (c) respectively, with the same number of capsules in the tank and in each layer. As can be seen, in the HCP and FCC layouts, the three-dimensional arrangements consisted of stacks of packing layers that were closer to each other, in which any three adjacent spheres composed an equilateral triangle. In other words, each sphere had 12 spheres contacting it tangentially. The number of tangential spheres of each capsule in the ADL packing was only eight. It was noted that the height of FCC and HCP packing was 316 mm while the height of ADL packing was 378 mm.

The PCM selected for the present study was a composite organic PCM, capric acid – lauric acid – oleic acid (CA-LA-OA), which has an appropriate phase change temperature for cold storage of air-conditioning systems (Wang et al., 2013). This PCM was self-developed and has manifested excellent thermal performance in a former study (Wang et al., 2019). Since the phase change of the PCM proceeded within a small temperature range, the influence of the slightly varied density and thermal conductivity on the phase change process was assumed negligible. The thermal-physical properties were treated as temperature independent as listed in **Table 1** (Guo et al., 2019; Wang et al., 2019). Water was selected as the HTF, which had a constant flowrate of 100 $L \cdot h^{-1}$ and a constant inlet temperature of = 7 °C. The initial temperature of the packed bed was uniform and set as = 22 °C.

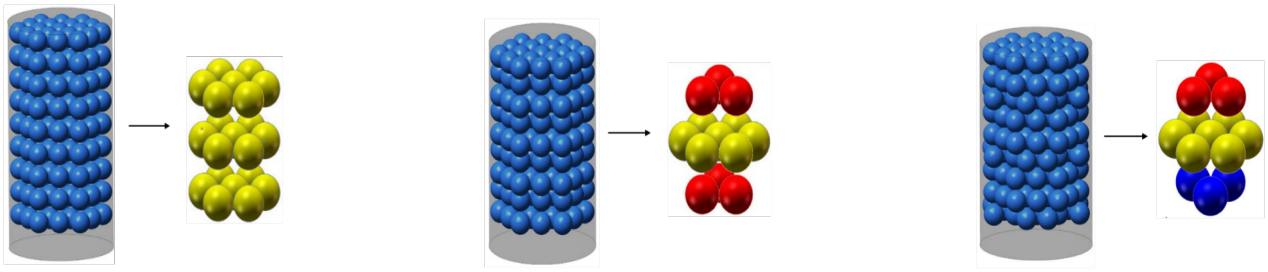

(a) (b) (c)

Fig. 1. Schematic of packed-bed cold storage: (a) ADL layout, (b) HCP layout, and (c) FCC layout

Table 1. Thermal-physical properties of the PCM and HTF

Material	state	ρ ($kg \cdot m^{-3}$)	c ($J \cdot kg^{-1} \cdot K^{-1}$)	k ($W \cdot m^{-1} \cdot K^{-1}$)	T (°C)	ΔH ($kJ \cdot kg^{-1}$)
C-L/O PCM	solid	845.1	1825	0.145	10.5	109.2
	liquid	839.7	2214	0.141	14.5	
HTF (water)	liquid	999.7	4193	0.58	-	-

2.2. Governing equations and numerical methods

In this work, a three-dimensional simulation model was established to describe the transient phase change process accompanied by the forced convection of HTF. The following assumptions were made:

1) The flow in the packed bed is steady and incompressible;

2) The thermal resistance of capsule shell is ignored considering that the capsule shell was set as thin as 1 mm and the shell thermal conductivity was 2.20 $W \cdot m^{-1} \cdot K^{-1}$, the effect of which was proven negligible (Wang et al., 2013);

3) The envelope is modeled as a rigid layer, and the effect of deformation is ignored in the simulation as Reynolds number is so low that the fluid can hardly cause any deformation of capsules;

4) PCM is homogeneous and isotropic;

5) Natural convection inside PCM capsules is neglected due to the small temperature difference ($\Delta T = 15°C$) between HTF and PCM, minimal density variation (~0.6%) between solid and liquid phases, and the conduction-dominated regime in small capsules (radius = 20 mm). This assumption is further justified by the low Rayleigh number ($Ra < 10^3$), which suppresses buoyancy-driven flows, as corroborated by prior studies (Ismail & Henríquez, 2000; Kenisarin et al., 2020; Sheikholeslami, 2018);

6) Gravitational force, as well as other external body forces, are neglected.

Based on the assumptions, for HTF the conservation equations of mass, momentum and energy are formulated as follows:

$$\frac{\partial(u_i)}{\partial x_i} = 0 \tag{1}$$

$$\rho_f \frac{\partial u_i}{\partial t} + \rho_f \frac{\partial}{\partial x_j}(u_i u_j) = -\frac{\partial P}{\partial x_i} + \mu_f \frac{\partial^2 u_i}{\partial x_j \partial x_j} \tag{2}$$

$$\rho_f c_f \frac{\partial T_f}{\partial t} + u_i \rho_f c_f \frac{\partial T_f}{\partial x_i} = k_f \frac{\partial^2 T_f}{\partial x_i \partial x_i} \tag{3}$$

where T_f is the temperature of the fluid, and k_f is the fluid thermal conductivity, and i represents a spatial coordinate direction in a Cartesian coordinate system.

For PCM, the enthalpy method was adopted to express the phase change process, by which one does not need to track the movement of solid-liquid phase interface during solidification/melting. The total enthalpy H consists of the sensible enthalpy h and the latent heat ΔH:

$$H = h + \Delta H \tag{4}$$

$$h = h_{ref} + \int_{T_{ref}}^{T} c_p \mathrm{d}T \tag{5}$$

$$\Delta H = \gamma L \tag{6}$$

where h_{ref} and T_{ref} are the reference enthalpy and temperature of the PCM, while c_p and L represent the specific heat and the latent heat of PCM, respectively. The liquid fraction γ is defined in Eq. (7) as:

$$\gamma = \begin{cases} 0 & (T_p < T_{solidus}) \\ \frac{T_p - T_{solidus}}{T_{liquidus} - T_{solidus}} & (T_{solidus} < T_p < T_{liquidus}) \\ 1 & (T_p > T_{liquidus}) \end{cases} \tag{7}$$

As a result, the energy equation for the PCM region is formulated as:

$$\rho_p \frac{\partial H}{\partial t} = k_p \frac{\partial^2 T_p}{\partial x_i \partial x_i} \tag{8}$$

where T_p is the temperature of the PCM and k_p is the PCM thermal conductivity.

The Reynolds number for this model, as Eq. (9) shows, is based on the interstitial velocity v_i and the pore-scale hydraulic diameter d_h of the packed bed (Yang et al., 2010).

$$Re_h = \frac{\rho_f v_i d_h}{\mu_f} \tag{9}$$

where ρ_f and μ_f are the density and dynamic viscosity of water, respectively, while the interstitial velocity v_i and the pore-scale hydraulic diameter d_h are defined by Eq.10 and Eq.11 respectively:

$$v_i = \frac{v_s}{\varphi} \tag{10}$$

where v_s is the inlet flow velocity, and φ is the porosity of the packed bed, that is also the proportion of space taken by HTF in the packed bed. The detailed φ values of ADL, HCP and FCC are 39.5%, 26.0% and 26.0%.

$$d_h = 4\frac{\varphi}{1-\varphi} \cdot \frac{V_p}{A_p} \tag{11}$$

where V_p and A_p are the volume and surface area of the capsule.

The surface average Nusselt number is defined as:

$$Nu_{aver} = \frac{q_s d_h}{(\overline{T_f} - \overline{T_s}) k_f} \tag{12}$$

where q_s is the heat flux of the active ball; $\overline{T}_f$ is the volume average temperature of HTF; and $\overline{T}_s$ is the surface average temperature of the active ball.

As for PCM packed beds, both pressure drop and heat transfer contribute to the thermal efficiency and they should be taken into account simultaneously. The improvement of heat transfer is usually at the cost of increased pressure drop. To evaluate the heat transfer performance considering both factors, the thermal performance factor to evaluate the heat transfer enhancement in the work (Gong et al., 2015) is defined below:

$$\mathrm{JF} = \left(\frac{Nu}{Nu_{ADL}}\right) / \left(\frac{\Delta p/L}{(\Delta p/L)_{ADL}}\right)^{1/3} \qquad (13)$$

where Nu_{ADL} and $(\Delta p / L)_{ADL}$ are respectively the Nusselt number and pressure drop of the ADL packing.

2.3. Meshing and implementation

The collinear geometric packing configuration of spherical capsules brings about point contacts in the form of sphere-sphere and sphere-wall interaction in the packed bed, where the mesh quality tends to be poor. Therefore, four methods, i.e. reducing, overlapping, caps and bridges, have been proposed in the literature to modify the contact point (Rebughini et al., 2016). Reported by Calis et al. (Calis et al., 2001), the reducing method, in which the spheres are stacked with very small gaps (1% of capsule outer radius) without contacting, was employed in the present study. The unstructured grids with tetrahedral elements were adopted for mesh generation in the domain due to their complicated geometric structures. **Fig. 2** shows a typical mesh distribution, where the grids near spherical surfaces are intensified.

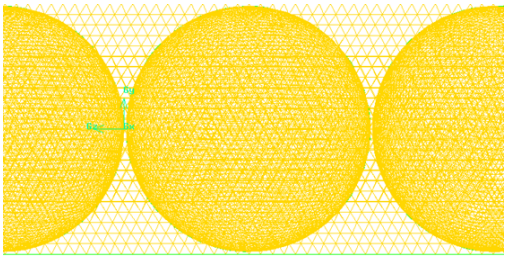

Fig. 2. Computational grid of the ADL layout model

The modelling was performed using the commercial software of ANSYS Fluent 18.0. The Reynolds numbers in the present study ranged from 1 to 200. The Energy model was turned on, and the steady-state laminar flow model was used as the momentum equation for this simulation. The SIMPLE algorithm was adopted for the pressure-velocity coupling. The Green-Gauss cell-based scheme was applied for the gradients, the stand discretization scheme was imposed on the pressure equation, and the second-order upwind scheme was selected for the momentum and energy equations. The convergence criteria were determined by monitoring the convergence residual for the continuity, momentum, and energy equations, which are set to 10^{-3}, 10^{-6}, and 10^{-6}, respectively.

2.4. Initial and boundary conditions

For the physical model of the packed-bed cold storage tank, the computation domains consisted of both the PCM capsules and the HTF. The initial temperature, T_{ini} for the whole packed bed was 22 °C and the initial velocity of HTF, u_{ini}, was 0. The coupled thermal boundaries were imposed on capsule surfaces in these cases. The inlet temperature, T_{in}, was set to 7 °C and a wide range of Reynolds numbers from 1 to 200 were investigated. The pressure condition of 0 Pa gauge backflow pressure was applied at the outlet. All the surfaces were set as no-slip walls.

3. Grid independence test and model validation

3.1. Independence of model grid and time step

Prior to iterative computations, grid size and time step convergence were checked. The total pressure drop and transient liquid fraction were selected as two typical metrics to test three different mesh sizes and time steps for the case of the packed-bed model with ADL layout. **Table 2** reveals the variations of the two metrics for the case among different mesh sizes and time steps. It can be recognized that a grid size of approximately 300000 cells and a time step of 0.1 s, which satisfied 0.8 of maximum skewness with a low aspect ratio, can be an ideal option considering both the accuracy and computational time. Similarly, the mesh sizes and time steps for other cases were examined. The corresponding mesh quality was also tested on the condition of no more than 0.85 of maximum skewness and 5.0 of maximum aspect ratio. The total numbers of grid elements for all the cases are listed in **Table 3**.

3.2. Experimental validation

Experimental tests were performed to validate the mathematical model. As shown in **Fig. 3**, the main experimental system consisted of a thermostated water bath and a chilled-water packed-bed cold storage tank. The cold storage tank was placed horizontally, and water that served as HTF was pumped to the inlet during the charging process. Nine layers with 19 capsules in each layer were packed in the storage tank. The PCM capsules were filled with composite C-L/O PCM. The capsule diameter and capsule wall thickness were 20 mm and 0.3 mm, respectively. The storage tank was insulated with a 4-cm rubber foam insulation layer.

To log water temperature and PCM temperature variation, 28 PT100 temperature sensors were fixed at different bed heights and seven-layer PT100 temperature sensors were equidistantly placed in the packed bed. At each layer, 4 PT100 temperature sensors were used to monitor HTF temperature and PCM temperature at the center of

Table 2. Grid size and time step independence test result for the packed-bed model with ADL layout

Number of cells	Time step (s)	Δp_{total}(Pa/m)	Liquid fraction		
			1000 s	5000 s	10000 s
1,035,976	0.1	0.0455	0.8592	0.3825	0.1312
1,223,391	0.1	0.0461	0.8578	0.3807	0.1305
1,979,355	0.1	0.0464	0.8577	0.3796	0.1301
1,223,391	0.05	0.0461	0.8578	0.3812	0.1307
1,223,391	0.1	0.0461	0.8578	0.3807	0.1305
1,223,391	0.2	0.0462	0.8578	0.3789	0.1296

Table 3. Grid size and time step independence test result for different models

Case	ADL	HCP	FCC
Number of grid elements	1,223,391	3,003,764	3,006,938
Time step (s)	0.1	0.1	0.1

the spherical capsules. The first layer near the bottom of the bed and the last layer near the top of the bed were designated as the inlet and outlet of the packed bed. A rotameter with an accuracy of ±4% was employed to monitor the flow rate. All the PT100 sensors, with an accuracy of ±0.15 °C, were calibrated using the thermostatic water bath. The temperature was logged every 30 s by the Keithley 2700 data acquisition system.

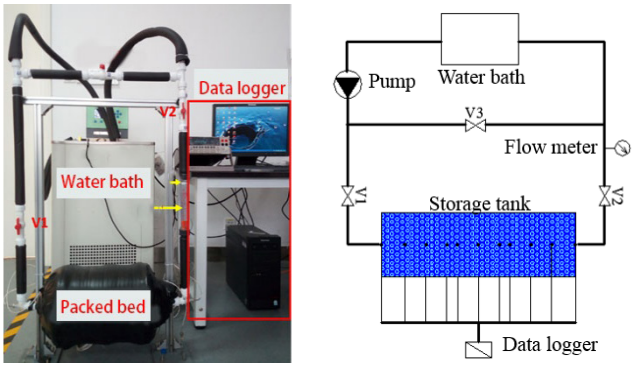

(a) (b)

Fig. 3. Experimental setup: (a) photo of the experimental setup; (b) schematic of the experimental setup

Numerical predicted time-dependent variations of HTF and PCM temperature were compared with the experimental data. The flow rate was 100 L h^{-1} and the inlet temperature was 7 °C. Root mean square error (RMSE) and Mean Absolute Percentage Error (MAPE) were used to evaluate the deviations between the simulation results and experimental data.

$$\mathrm{RMSE} = \sqrt{\frac{1}{n}\sum_{\tau=1}^{n}(T_\tau - T_\tau')^2} \quad (4)$$

$$\mathrm{MAPE} = \frac{1}{n}\sum_{\tau=1}^{n}\left|\frac{T_\tau - T_\tau'}{T_\tau'}\right| \quad (5)$$

where n is the total number of data compared. T_τ and T_τ' are the simulated and experimental temperature, respectively, recorded at the time step of τ.

The comparison of experimental and simulated PCM and HTF temperatures are shown in **Fig. 4**. The simulation results are in good agreement with the experimental data, as the RMSE and MAPE for the PCM temperature are observed to be 0.89 °C and 5.49%, and the corresponding values for HTF temperature are 0.41 °C and 2.04%.

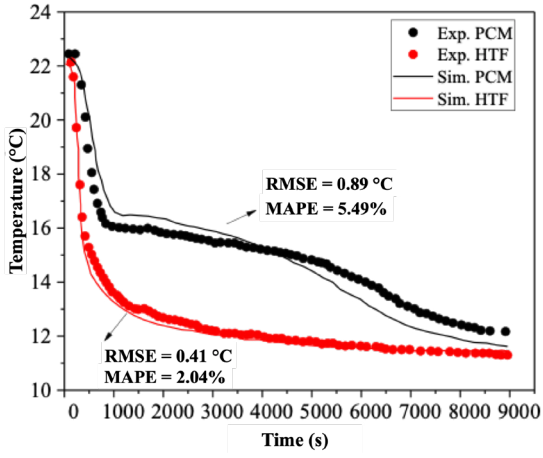

Fig. 4. Comparisons of experimental data with numerical results

4. Results and discussion

4.1. Effects of the packing configuration on the packed bed

Considering the compactness, compared with the ADL packing, the theoretical PCM packing density for HCP and FCC layouts was raised by 22.5%, thus considerably saving the footprint of the packed bed. Furthermore, the packing density compares favorably with other recent strategies aimed at improving thermal performance. For example, in a study involving hydrate-based carbon capture using packed RBC-shaped capsules (Zhang et al., 2024), the reported packing density was 64.3%, which is approximately 13% lower than that of the HCP and FCC layouts. In addition, studies utilizing flow-guiding conduits have generally resulted in lower packing densities due to the volume occupied by internal structures within the packed bed (Guo et al., 2019).

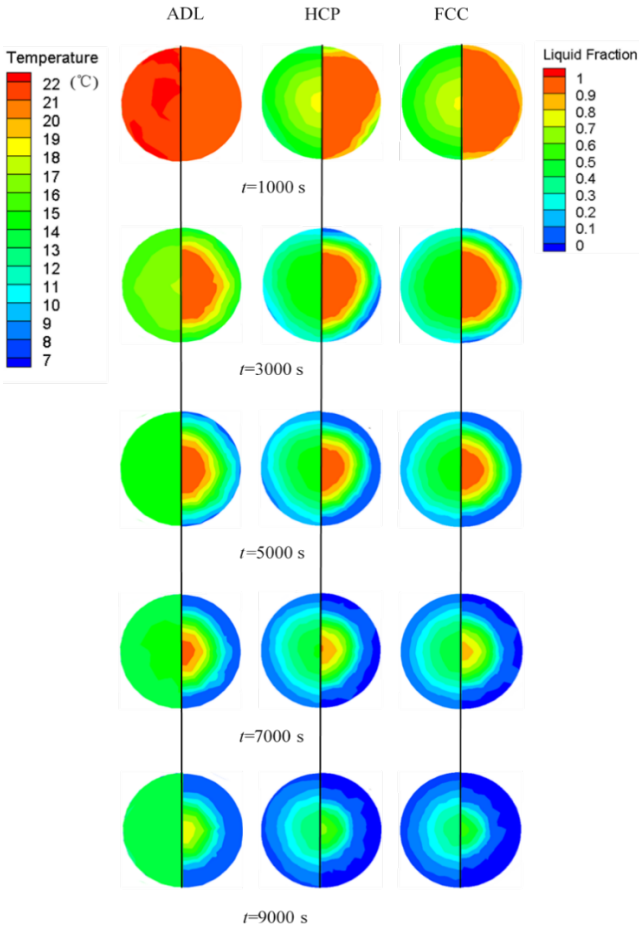

Fig. 5. Temperature gradient (left half) and liquid fraction distribution (right half) of the capsule cross section ($z = 0$) of different packed-bed model packing configurations

Based on the investigation of flow and heat transfer mechanisms of different packing configurations in the model of a whole packed bed, a practical analysis of the charging rate across the different packed beds was carried out. The PCM mass and inlet HTF flowrate (100 L/h) were identical for all the packing configurations to make sure that the layout is the only variable. All the capsules in the packed bed were active to exchange heat with HTF. The parameters and boundary conditions of the packed beds are depicted in Section 2.1. The capsule in the center of the fifth layer was selected as an example to represent the charging process of the packing configuration. **Fig. 5** depicts the temperature gradient (left half) and liquid fraction distribution (right half) of the cross section (z = 0) of the selected sphere.

The comparisons are implemented at several typical time instants. For t = 1000 s, the temperature was at a uniform level of 21 °C throughout the sphere in ADL. The heat transfer was attributed to pure heat conduction. In regard to the other two packed beds, the isotherms presented as a series of concentric circles. Regarding the phase change process, the liquid fraction distribution in FCC was more homogeneous than in HCP. This means that the melting front in FCC progressed more uniformly across the sphere, with smaller local variations in the liquid fraction, whereas HCP showed greater disparities in the liquid fraction, indicating less uniform phase change behavior. At t = 3000 s, PCM in ADL began to solidify, while its solidification rate was the slowest. The phase change process in the center of spheres lagged behind other domains due to the highest thermal resistance. Beyond t = 7000 s, almost all the PCM in the sphere of HCP and FCC began to solidify; however, a small portion of PCM at the sphere center of ADL did not begin to solidify before t = 9000 s.

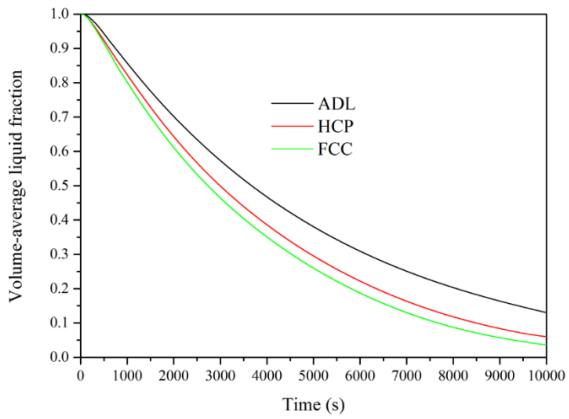

Fig. 6. Variation of PCM volume-average liquid fraction of different packed-bed model packing configurations

A key index, the volume-average liquid fraction of PCM, is employed to assess the thermal performance of each packed bed. As the volume-average liquid fraction declines from 1 to 0, it indicates that PCM in the packed bed gradually changes its phase state towards the complete solid. **Fig. 6** shows the variation of PCM volume-average liquid fraction in different cases. It was observed that the liquid fraction distribution in each packed bed presented a similar downtrend, while the duration of the charging process decreased in the order of ADL > HCP > FCC. To analyze the peculiarity of transient solidification rate quantitatively, the charging time is defined in this study as the minimum time required for PCM in the packed bed to reach 90% phase change. It was revealed that HCP and FCC saved up to 21.4% and 29.0% of charging time, respectively, in comparison with that of ADL. The results

suggest that the overall heat transfer capability of HCP and FCC is greatly improved during solidification and the increased extent of FCC is more dramatic.

To figure out the heat transfer performance during the charging period in each packed bed, the variations of charging rates of different cases are shown in **Fig. 7**. It was displayed that the cold storage process in diversely packed beds could be divided into three successive stages. In the initial sensible cooling stage (0–300 s), the large temperature gradient between the HTF and PCM drives rapid sensible heat extraction. Convective heat transfer at the capsule surfaces dominates, with no phase change occurring. The charging rate rises sharply to a peak value (~50 W difference between FCC and ADL at t = 300 s), reflecting enhanced convective efficiency in structured layouts (FCC/HCP) due to reduced flow channeling. In the latent heat release stage (300–4500 s), solidification initiates at the capsule periphery as PCM temperatures reach the phase change point. Latent heat release stabilizes local temperatures, while thermal resistance from the growing solid layer gradually reduces the charging rate. The FCC layout accelerates this stage by minimizing void spaces, which enhances HTF-PCM contact and convective heat transfer. In the final sensible cooling stage (t > 4500 s), residual heat is removed via conduction through the solid phase. The diminished temperature gradient results in a slow, monotonic decline in charging rates. Notably, the charging rate order reverses beyond 4500 s, as ADL's looser packing allows marginally better conduction in the fully solidified regime.

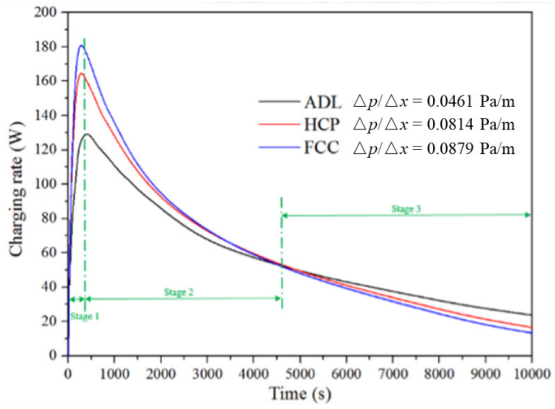

Fig. 7. Transient variations of charging rate and pressure drop of different packed-bed model packing configurations

However, despite improving heat transfer rate, the pressure drop across the whole packed bed inevitably increased in the cases of HCP and FCC. The time-independent flow of HTF in the packed resulted in the pressure drops of ADL, HCP and FCC of 0.0461, 0.0814 and 0.0879 Pa m^{-1}, respectively. I.e., the optimized packing configurations played a significant role in enhancing heat transfer efficiency of the whole packed bed, however at the cost of increased pressure drop. While FCC/HCP layouts incur higher pressure drops, their superior thermal performance and compactness result in net energy savings and reduced system footprint.

A comparative analysis of different packed bed configurations in terms of energy storage density, heat transfer enhancement, and pressure drop characteristics is shown in **Table 4**. Studies on grille-sphere composite packed beds (GSCSPBs) have shown that their particle-to-fluid heat transfer coefficient is 94% higher than that of simple cubic (SC) packing, reaching approximately 76% of the heat transfer observed in randomly packed beds (Wang et al., 2017). Meanwhile, composite structured packed beds (CSPBs) exhibit improved heat transfer due to enhanced flow distribution and increased fluid-solid contact areas while maintaining a lower pressure drop than randomly packed beds (Romkes et al., 2003). In contrast, the HCP and FCC layouts provide a high packing density (~74%), which translates to increased energy storage capacity, while also offering structured conduction pathways for thermal enhancement. Although GSCSPBs and CSPBs focus on optimizing heat transfer and flow resistance, their energy storage density is generally lower, making HCP and FCC configurations more suitable for applications prioritizing thermal storage efficiency.

4.2. Normalized charging efficiency factor of packed bed cold storage

The newly defined normalized charging efficiency factor, β_{charge}, is formulated in Eq (16). Differing from the overall thermal performance factor, this metric compares the cooling capacity storage gain to the pump hydraulic power. It is defined as the ratio of the average charging rate (the gain) to the (modified) pressure loss (the cost). Due to the fact that the pump power consumption usually accounts for a small portion of the chiller power consumption, the ratio between the two is used to modify the weight of pressure loss as an exponential:

$$\beta_{charge} = \frac{E_{charge}/\tau}{\Delta p^{Q_{pump}/Q_{charge}}} = \frac{E_{charge}/\tau}{\Delta p^{(\frac{q\Delta p}{1000\eta})/(\frac{E_{charge}/\tau}{COP})}} \quad (16)$$

where E_{charge} (J) is the overall cooling capacity of the packed-bed cold storage; COP refers to the coefficient of performance of the chiller; q is the HTF flowrate (L s^{-1}); Δp is the overall pressure loss of the packed-bed cold storage (Pa); τ and η are the time and the lumped pump and motor efficiency (%), respectively. The pump electric power, Q_{pump} (W) may be calculated using the formula below (Karassik, 2001).

$$Q_{pump} = \frac{q\Delta p}{1000\eta} \quad (17)$$

The simulation result of charging time and pressure loss are summarized in **Table 5** for the case of ADL, HCP and FCC. The total cooling capacity was 576,304 J. COP in this study was set at 5, and the pump efficiency and motor efficiency were both 0.85. They were all the same for the three cases. The charging time of the whole packed-bed cold storage was reduced by 21.4% and 29.0% by applying HCP and FCC configurations, respectively, in comparison to ADL. Based on the aforementioned flow

Table 4. Comparative Analysis of Packing Configurations

Packing Configuration	Energy Storage Density	Heat Transfer Enhancement	Pressure Drop Characteristics
Hexagonal Close-Packed (HCP)	High (≈74% packing density)	Moderate; improved conduction pathways due to ordered structure.	Moderate; increased contact points may lead to higher pressure drop compared to less dense packings.
Face-Centered Cubic (FCC)	High (≈74% packing density)	Moderate; similar to HCP with efficient conduction pathways.	Moderate; structured arrangement balances pressure drop and heat transfer.
Composite Structured Packed Beds (CSPBs) (Romkes et al., 2003)	Moderate to High; specific values not detailed in literature	Enhanced; improved flow distribution and increased contact area between fluid and particles.	Reduced compared to randomly packed beds;
Grille-Sphere Composite Packed Beds (GSCSPBs) (Wang et al., 2017)	Moderate to High; specific values not detailed in literature	Significantly enhanced; studies report up to 94% higher heat transfer coefficients compared to simple cubic packing and achieving 76% of the heat transfer in randomly packed beds.	Lower than randomly packed beds

Table 5. Key performance metrics of the whole packed bed with three packing configurations

Packing configuration	Charging time (s)	Total pressure loss (Pa)	Energy storage density (%)	Pump power consumption (W)	Normalized charging efficiency factor
ADL	10.8×10^3	0.0166	60.5	8.39	68.0
HCP	8.49×10^3	0.0245	74.1	6.70	83.5
FCC	7.67×10^3	0.0265	74.1	6.48	91.6

parameters, the pump power consumption was calculated considering both pressure loss and gravity. The results showed that FCC also consumes the lowest pumping power due to the shortest charging time and small height. The normalized charging efficiency factor, as defined, compares the rate of charging with the cost of pumping power. From the results, FCC achieved the best efficiency (34.7% higher than that of ADL), followed by HCP (22.8% higher than that of ADL). Dense packings are better performing in all the metrics than loose capsule packings.

5. Conclusions

In the present paper, two new packing configurations of capsules, FCC and HCP, were designed for the PCM packed-bed cold storage to increase the storage density. Through simulation conducted in ANSYS Fluent 18.0, the flow characteristics and heat transfer performance of the packed bed with various capsule packings were investigated and compared at different Reynolds numbers. The conclusions are as follows:

(1) HCC and FCC are both three-dimensional dense packings, which plays a vital role in saving space volume and manufacturing costs for PCM packed beds. By comparison, the theoretical PCM packed density of HCP and FCC packing is 22.5% larger than that of conventional ADL packing.

(2) Compared with other packings, FCC, despite its improved heat transfer performance, inevitably exhibits the increased pressure drop across the whole packed bed. The pressure drop of ADL, HCP and FCC is 0.0461, 0.0814 and 0.0879 Pa m^{-1}, respectively.

(3) As for PCM packed beds, the charging time of the packed-bed cold storage is reduced by 21.4% and 29.0% by applying HCP and FCC configurations, respectively, compared to ADL. It is found that FCC bed has superior heat transfer rates due to promoted convection in HTF.

(4) A new metric, normalized charging efficiency factor, was defined for the first time, comparing the cooling capacity storage gain to the pump hydraulic power. The best value was found for FCC (34.7% higher than that of ADL), followed by HCP (22.8% higher than that of ADL).

While the FCC and HCP layouts demonstrate superior thermal performance and energy density for PCM cold storage, their commercial adoption faces challenges, including manufacturing complexity, scalability constraints and maintenance challenges. However, the principles of structured packing offer valuable insights transferable to diverse fields. Applications such as solar thermal energy storage, catalytic and biomedical reactors, can leverage optimized packing geometries to enhance heat transfer, reduce footprint, and balance hydraulic-thermal trade-offs.

Acknowledgements

This work was supported by the National Natural Science Foundation of China under contract No. 51776117.

Reference

Bindra, H., Bueno, P., Morris, J. F., & Shinnar, R. (2013). Thermal analysis and exergy evaluation of packed bed thermal storage systems. *Applied Thermal Engineering*, *52*(2), 255-263.

Calis, H., Nijenhuis, J., Paikert, B., Dautzenberg, F., & Van Den Bleek, C. (2001). CFD modelling and experimental validation of pressure drop and flow profile in a novel structured catalytic reactor packing. *Chemical Engineering Science*, *56*(4), 1713-1720.

Chen, L., Lee, W., & Lee, J. (2017). Analysis of the thermal field and heat transfer characteristics of pebble beds packed in a face-centered cubic structure. *Applied Thermal Engineering*, *121*, 473-483.

Chen, L., Wang, C., Moscardini, M., Kamlah, M., & Liu, S. (2019). A DEM-based heat transfer model for the evaluation of effective thermal conductivity of packed beds filled with stagnant fluid: Thermal contact theory and numerical simulation. *International Journal of Heat and Mass Transfer*, *132*, 331-346.

Cheng, X., & Zhai, X. (2017). Thermal performance analysis of a novel PCM capsule in red blood cell shape. *Applied Thermal Engineering*, *120*, 130-137.

Cheng, X., & Zhai, X. (2018a). Thermal performance analysis and optimization of a cascaded packed bed cool thermal energy storage unit using multiple phase change materials. *Applied Energy*, *215*, 566-576.

Cheng, X., & Zhai, X. (2018b). Thermal performance analysis of a cascaded cold storage unit using multiple PCMs. *Energy*, *143*, 448-457.

Cheng, X., Zhai, X., Wang, X., & Lin, P. (2020). Numerical study of forced convection over phase change material capsules in a traditional spherical shape and a biomimetic shape. *Journal of Energy Storage*, *31*, 101526.

Das, S., Deen, N. G., & Kuipers, J. (2017). A DNS study of flow and heat transfer through slender fixed-bed reactors randomly packed with spherical particles. *Chemical Engineering Science*, *160*, 1-19.

Diao, Y., Liang, L., Zhao, Y., Wang, Z., & Bai, F. (2019). Numerical investigation of the thermal performance enhancement of latent heat thermal energy storage using longitudinal rectangular fins and flat micro-heat pipe arrays. *Applied Energy*, *233*, 894-905.

Fleuchaus, P., Godschalk, B., Stober, I., & Blum, P. (2018). Worldwide application of aquifer thermal energy storage–A review. *Renewable and Sustainable Energy Reviews*, *94*, 861-876.

Gielen, D., Boshell, F., Saygin, D., Bazilian, M. D., Wagner, N., & Gorini, R. (2019). The role of renewable energy in the global energy transformation. *Energy strategy reviews*, *24*, 38-50.

Gong, B., Wang, L.-B., & Lin, Z.-M. (2015). Heat transfer characteristics of a circular tube bank fin heat exchanger with fins punched curve rectangular vortex generators in the wake regions of the tubes. *Applied Thermal Engineering*, *75*, 224-238.

Grosso, G., & Parravicini, G. P. (2013). *Solid state physics*. Academic press.

Guo, X., & Dai, R. (2010). Numerical simulation of flow and heat transfer in a random packed bed. *Particuology*, *8*(3), 293-299.

Guo, Z., Sun, Z., Zhang, N., & Ding, M. (2019). Influence of confining wall on pressure drop and particle-to-fluid heat transfer in packed beds with small D/d ratios under high Reynolds number. *Chemical Engineering Science*, *209*, 115200.

Guo, Z., Sun, Z., Zhang, N., Ding, M., Bian, H., & Meng, Z. (2019). Computational study on fluid flow and heat transfer characteristic of hollow structured packed bed. *Powder Technology*, *344*, 463-474.

Guo, Z., Sun, Z., Zhang, N., Ding, M., & Liu, J. (2017). Pressure drop in slender packed beds with novel packing arrangement. *Powder Technology*, *321*, 286-292.

Guo, Z., Sun, Z., Zhang, N., Ding, M., & Shi, S. (2019). CFD analysis of fluid flow and particle-to-fluid heat transfer in packed bed with radial layered configuration. *Chemical Engineering Science*, *197*, 357-370.

Guo, Z., Sun, Z., Zhang, N., Ding, M., & Zhou, Y. (2019). Influence of flow guiding conduit on pressure drop and convective heat transfer in packed beds. *International Journal of Heat and Mass Transfer*, *134*, 489-502.

Halkarni, S. S., Sridharan, A., & Prabhu, S. (2016). Estimation of volumetric heat transfer coefficient in randomly packed beds of uniform sized spheres with water as working medium. *International Journal of Thermal Sciences*, *110*, 340-355.

Halkarni, S. S., Sridharan, A., & Prabhu, S. (2017). Measurement of local wall heat transfer coefficient in randomly packed beds of uniform sized spheres using infrared thermography (IR) and water as working medium. *Applied Thermal Engineering*, *126*, 358-378.

Helm, C., & Mier, M. (2019). On the efficient market diffusion of intermittent renewable energies. *Energy Economics*, *80*, 812-830.

Hu, Y., Wang, J., Yang, J., Mudawar, I., & Wang, Q. (2019). Experimental study of forced convective heat transfer in grille-particle composite packed beds. *International Journal of Heat and Mass Transfer*, *129*, 103-112.

Hu, Y., Yang, J., Wang, J., & Wang, Q. (2018). Investigation of hydrodynamic and heat transfer performances in grille-sphere composite pebble beds with DEM-CFD-Taguchi method. *Energy*, *155*, 909-920.

Ismail, K., & Henríquez, J. (2000). Solidification of PCM inside a spherical capsule. *Energy Conversion and Management*, *41*(2), 173-187.

Jia, X., Zhai, X., & Cheng, X. (2019). Thermal performance analysis and optimization of a spherical PCM capsule with pin-fins for cold storage. *Applied Thermal Engineering*, *148*, 929-938.

Karassik, I. J. (2001). *Pump handbook*.

Kenisarin, M. M., Mahkamov, K., Costa, S. C., & Makhkamova, I. (2020). Melting and solidification of PCMs inside a spherical capsule: A critical review. *Journal of Energy Storage*, *27*, 101082.

Lee, D.-Y., & Chung, B.-J. (2019). Variations of forced convection heat transfer of packed beds according to the heated sphere position and bed height. *International Communications in Heat and Mass Transfer*, *103*, 64-71.

Li, B., Zhai, X., & Cheng, X. (2019). Thermal performance analysis and optimization of multiple stage latent heat storage unit based on entransy theory. *International Journal of Heat and Mass Transfer*, *135*, 149-157.

Li, T., Xu, J., Wu, D., He, F., & Wang, R. (2019). High energy-density and power-density thermal storage prototype with hydrated salt for hot water and space heating. *Applied Energy*, *248*, 406-414.

Qian, P., Wang, J., Wu, Z., Yang, J., & Wang, Q. (2019). Performance comparison of methane steam reforming in a randomly packed bed and a grille-sphere composite packed bed. *Energy Conversion and Management*, *193*, 39-51.

Rebughini, S., Cuoci, A., & Maestri, M. (2016). Handling contact points in reactive CFD simulations of heterogeneous catalytic fixed bed reactors. *Chemical Engineering Science*, *141*, 240-249.

Romkes, S., Dautzenberg, F., Van den Bleek, C., & Calis, H. (2003). CFD modelling and experimental validation of particle-to-fluid mass and heat transfer in a packed bed at very low channel to particle diameter ratio. *Chemical Engineering Journal*, *96*(1-3), 3-13.

Sheikholeslami, M. (2018). Numerical modeling of nano enhanced PCM solidification in an enclosure with metallic fin. *Journal of Molecular Liquids*, *259*, 424-438.

Sobes, V., Forget, B., & Kadak, A. (2011). Individual pebble temperature peaking factor due to local pebble arrangement in a pebble bed reactor core. *Nuclear engineering and design*, *241*(1), 124-133.

Tian, X.-W., Xu, S.-M., Sun, Z.-H., Wang, P., Xu, L., & Zhang, Z. (2018). Experimental study on flow and heat transfer of power law fluid in structured packed porous media of particles. *Experimental Thermal and Fluid Science*, *90*, 37-47.

Toghraie, D., Afrand, M., Zadeh, A. D., & Akbari, H. A. (2018). Numerical investigation on the flow and heat transfer of a multi-lobe particle and equivalent spherical particles in a packed bed with considering the wall effects. *International Journal of Mechanical Sciences*, *138*, 350-367.

Wang, J., Guo, Q., Yang, J., Liu, Y., & Wang, Q. (2017). Experimental study of convective heat transfer in grille-sphere composite structured packed bed. *Energy Procedia*, *105*, 4782-4787.

Wang, J., Yang, J., Cheng, Z., Liu, Y., Chen, Y., & Wang, Q. (2018). Experimental and numerical study on pressure drop and heat transfer performance of grille-sphere composite structured packed bed. *Applied Energy*, *227*, 719-730.

Wang, P., Zhao, P., Xu, W., Wang, J., & Dai, Y. (2019). Performance analysis of a combined heat and compressed air energy storage system with packed bed unit and electrical heater. *Applied Thermal Engineering*, *162*, 114321.

Wang, X., Zhai, X., Wang, T., Wang, H., & Yin, Y. (2013). Performance of the capric and lauric acid mixture with additives as cold storage materials for high temperature cooling application. *Applied Thermal Engineering*, *58*(1-2), 252-260.

Yang, J., Wang, Q., Zeng, M., & Nakayama, A. (2010). Computational study of forced convective heat transfer in structured packed beds with spherical or ellipsoidal particles. *Chemical Engineering Science*, *65*(2), 726-738.

Yeboah, S., & Darkwa, J. (2019). Experimental investigations into the adsorption enhancement in packed beds using Z-Annular flow configuration. *International Journal of Thermal Sciences*, *136*, 121-134.

Zenner, A., Fiaty, K., Bellière-Baca, V., Rocha, C., Gauthier, G., & Edouard, D. (2019). Effective heat transfers in packed bed: Experimental and model investigation. *Chemical Engineering Science*, *201*, 424-436.

Zhai, X., Cheng, X., Wang, C., & Wang, R. (2015). Experimental investigation and performance analysis of a fin tube phase change cold storage unit for high temperature cooling application. *Energy and Buildings*, *89*, 9-17.

Zhang, Y., Zhang, Z., Lu, Y., Chalermsinsuwan, B., Wang, F., Zhang, H., & Wang, X. (2024). Efficient hydrate-based carbon capture system enabled by red blood cell inspired encapsulation. *Applied Energy*, *359*, 122784.

Engineering Power – *Bulletin of the Croatian Academy of Engineering* Vol. 19(3) 2024 – ISSN 1331-7210 (Print)
ISSN 2718-322X (Online)
Publisher: Croatian Academy of Engineering (HATZ), 28 Kačić Street, P.O. Box 14, HR-10000 Zagreb, Republic of Croatia
Editor-in-Chief: Prof. Vedran Mornar, Ph.D., President of the Academy
University of Zagreb, Faculty of Electrical Engineering and Computing
Editor: Prof. Bruno Zelić, Ph.D., Vice-President of the Academy
University of Zagreb, Faculty of Chemical Engineering and Technology
Guest-Editor: Prof. Neven Duić, Ph.D., University of Zagreb, Faculty of Mechanical Engineering and Naval Architecture
Activities Editor: Tanja Miškić Rogić
Editorial Board: Prof. Vedran Mornar, Ph.D., Prof. Vladimir Andročec, Ph.D., Prof. Bruno Zelić, Ph.D., Assoc. Prof. Mario Bačić, Ph.D., Prof. Neven Duić, Ph.D.
Editorial Board Address: Croatian Academy of Engineering (HATZ), "Engineering Power" – Bulletin of the Croatian Academy of Engineering, Editorial Board, 28 Kačić Street, P.O. Box 14, HR-10000 Zagreb, Republic of Croatia
E-mail: hatz@hatz.hr
Graphical and Technical Editor: Tiskara Zelina, Ltd., Zelina
Press: Tiskara Zelina, Ltd., Zelina
Circulation: 200